AN ABSTRACT OF THE THESIS OF

Don Tavolacci (Name) for the degree Master of Science (Degree)

in Mechanical Engineering (Major) presented on July 26, 1974 (Date)

Title: FLUID FORCES ON AND FLOW CONFIGURATIONS AROUND A CIRCULAR CYLINDER NEAR A PLANE BOUNDARY

Abstract approved: Redacted for Privacy

Dr. John H. Nath

The flow configurations around and the forces acting on a circular cylinder with its axis parallel to a nearby plane boundary and subjected to a uniform flow were investigated. The flow conditions, which were perpendicular to the cylinder axis and parallel to the plane boundary were investigated experimentally and theoretically. Flow visualization was achieved through the use of tiny air bubbles entrapted in the fluid to locate the stagnation point and point of separation of flow. Also, the configuration of the cylinder wake was observed. A force measuring device employing the use of strain-gauges was used to record the change in lift and drag as the cylinder neared the plane boundary.

The results showed that the drag and lift increased, and that the cylinder wake approximated that of an aerofoil configuration as the cylinder neared the plane boundary. In addition, as the cylinder approached the plane boundary, the top separation point of the

cylinder boundary layer moved towards the front of the cylinder, the bottom separation point moved towards the rear of the cylinder, and the front stagnation point moved downward. The boundary layer along the plane boundary was observed to separate at a position downstream of the test cylinder. This separation point position was determined to be a function of the distance between the cylinder and the plane boundary for a specific Reynolds number.

FLUID FORCES ON AND FLOW CONFIGURATIONS AROUND A CIRCULAR CYLINDER NEAR A PLANE BOUNDARY

by

Don Tavolacci

A THESIS

submitted to

Oregon State University

in partial fulfillment of
the requirements for the
degree of

Master of Science

July 1975

APPROVED:

Redacted for Privacy

Professor of Mechanical Engineering

in charge of major

Redacted for Privacy

Head of Department of Mechanical and Metallurgical Engineering

Redacted for Privacy

Dean of Graduate School

Date thesis is presented July 26, 1974

Typed by Pam Standiford for Don Tavolacci

ACKNOWLEDGEMENTS

For the guidance and advice that was given during the preparation and writing of this thesis, the author would like to express his gratitude and deep appreciation to Tokuo Yamamoto and John H. Nath.

This thesis was supported entirely by the National Oceanic and Atmospheric Administration (maintained by the U.S. Department of Commerce) institutional Sea Grant contract 4-3-158-4 at Oregon State University and the author would like to thank this institution for it's support.

TABLE OF CONTENTS

LIST OF ILLUSTRATIONS

LIST OF NOTATIONS

C_D	drag coefficient
C_L	lift coefficient
D	diameter of the cylinder, 2a
F_H	horizontal force per unit length of cylinder
F_V	vertical force per unit length of cylinder
H	channel water height, ft.
Re	Reynolds number, UD/γ
S	Strouhal number, nD/U
Q	channel flow rate, $ft^3/sec.$
U	velocity in x-direction
V	velocity in y-direction
W	complex potential, $\phi + q\ \psi$
a	radius of cylinder
e	gap between cylinder and bottom boundary
g	acceleration of gravity 32.2 ft/sec^2
i	$\sqrt{-1}$
m	strength of doublet
n	cyclic frequency
q_n	$((2s/a)-q_{n-1})^{-1}$, where $q_o = 0$, doublet position and strength parameter
s	distance from center of cylinder to bottom boundary
x	horizontal distance
z	vertical distance
Σ	summation

ϕ angle from horizontal axis of cylinder

γ kinematic viscosity of fluid

π 3.14159

u velocity, in x direction

ρ mass density of fluid

δ_1 displacement thickness $\int_{y=0}^{\infty} (1 - \frac{u}{U_\infty}) dy$

δ_2 momentum thickness $\int_{y=0}^{\infty} \frac{u}{U_\infty} (1 - \frac{u}{U_\infty}) dy$

τ_o shear stress $\mu (\frac{\partial u}{\partial y})_{y=0}$

μ viscosity of fluid

∇ gradient, $\frac{\partial}{\partial x}, \frac{\partial}{\partial y}, \frac{\partial}{\partial z}$

∇^2 Laplacean operator $\frac{\partial^2}{\partial x^2}, \frac{\partial^2}{\partial y^2}, \frac{\partial^2}{\partial z^2}$

FLUID FORCES ON AND FLOW CONFIGURATIONS AROUND A CIRCULAR CYLINDER NEAR A PLANE BOUNDARY

1.0 INTRODUCTION

Many ocean engineering structures are constructed of circular pipe sections. For the transportation of liquids, gases, or communication cable, circular structures are chiefly relied upon. The popularity of the circular form is due to its availability, high strength, and symmetrical nature. With such modern day dependence upon circular cylinders, one would assume that the knowledge of the fluid flow regimes around such elements would be complete. However, such is not the case.

Proven and reliable theories of the influence of the proximity of the ocean bottom on the hydrodynamic forces on a cylinder for a steady state condition are not completely known. Additional information is needed to verify experimental and theoretical data on flow configurations around and the forces acting on a cylinder whose axis is parallel to a plane boundary and which is subjected to a uniform flow that is perpendicular to the cylinder axis and parallel to the plane boundary. The writer hopes that this thesis will contribute to this needed fund of knowledge.

2.0 THEORETICAL AND REAL FLOW CONSIDERATIONS

2.1 Assumptions and Limits of the Potential Flow Theory

Certain assumptions have to be made in order to use potential flow theory to describe real fluid flow conditions. Physically, the shear stresses that exist in real fluid flow due to viscosity are neglected. For the case of incompressible, irrotational, frictionless flows, the flow velocity vector can be represented as the gradient of a potential that satisfies the Laplace equation as shown below.

$$\begin{aligned} \bar{q} &= -\nabla\phi \\ \nabla x\bar{q} &= 0 \\ \nabla^2\phi &= 0 \end{aligned} \qquad (1)$$

where ϕ = velocity potential

$\bar{q}$ = velocity vector

The potential flow theory is normally quite accurate where the general flow displays irrotational characteristics. Referring to Figure 1, the region designated as P can be included in this category. Other flow regimes outside boundary layer development and outside the separation regions also may display the characteristics of irrotational flow.

2.2 Real Fluid Flow Around a Cylinder

This section contains general information on fluid flow around cylinders that is pertinent to the problem at hand. More specific

information on how a nearby plane boundary influences the flow is given in section 2.3.

2.21 Boundary Layer Separation

Boundary layers exist for most real flow conditions. By definition, the boundary layer includes fluid near a boundary whose velocity is less than 99% of the potential flow velocity of that region and where the fluid in the boundary layer is flowing in the same general direction as the ambient fluid flow. Two necessary conditions must be present for boundary layer separation to exist, fluid viscosity and an adverse pressure gradient (2), (14). Classically, the beginning of the boundary layer separation is defined to occur where

$$\left.\frac{\partial u}{\partial y}\right|_{y=0} = 0 \qquad (2)$$

where u = fluid velocity parallel to the cylinder surface

y = axis perpendicular to the cylinder surface

Referring to Figure 1, within the boundary layer along the surface of the cylinder, the effect of viscosity will continually retard the fluid flow, which has a slow velocity near the cylinder surface compared with the free stream velocity. Thus the momentum of flow in the boundary layer will be smaller than for the ideal (frictionless) flow case. Looking at Figure 1, the boundary layer will thicken from point A to point B due to friction. In this region the pressure gradient is negative. From point B to point C, not only will friction be present, but an adverse pressure gradient exists due to the divergence of flow (i.e. the pressure gradient is positive). If the

small amount of momentum in the boundary layer is depleted while the fluid is overcoming the friction and pressure rise, the fluid particles are brought to rest. Downstream of the point of separation, reverse flow occurs because of the still existing adverse pressure gradient. Due to the reverse flow, the boundary layer separates from the surface of the cylinder.

2.22 Vortex Formation and Shedding and the Strouhal Number

For a cylinder in a free stream, vortex shedding and wake geometry are functions of the Reynolds number, (2), (6), (9), and (14). At a Reynolds number of less than one, the flow around a cylinder follows Stokes law as the streamlines essentially close behind the cylinder.

At Reynolds numbers around 10, laminar flow separation of the cylinder boundary layer occurs and two symmetric weak eddies form in the wake of the cylinder.

At a Reynolds number of approximately 100, one of the vortices breaks away from the cylinder, being washed downstream, which initiates a regular alternating pattern of vortex shedding. The von Karman's vortex street then forms.

For the range of Reynolds number of 10^3-10^5, the wake becomes more turbulent and the vortices diffuse soon after moving downstream as indicated in reference (12) and (13). The coefficient of drag has been found to be between approximately 0.9 and 1.3, (14), and the location of the laminar boundary layer separation point has been found to be between $\phi = 80^o$-85^o (14) for this range of Reynolds numbers.

At Reynolds numbers larger than 10^5, the flow in the cylinder boundary layer becomes turbulent to such a degree that the point of separation of the cylinder boundary layer moves downstream because of the added momentum gained by the turbulent boundary layer. The shift in the location of the separation point is directly responsible for a decrease in the wake area, thereby reducing the drag coefficient on the cylinder (2).

In real fluid flow, the existance of a wake behind a cylinder as described in section 2.2 for most Reynolds numbers is a well established fact. For flows between $40 < Re < 6 \times 10^5$, the cylinder wake has a tendency to oscillate perpendicular to the direction of flow due to the alternate shedding of vortices. Investigations of the periodicity of the wake by Strouhal (16) led to a non-dimensional number relating the diameter of the cylinder D, the stream velocity U, and the periodicity n as follows

$$S = nD/U \qquad (3)$$

The dependency of the Strouhal number upon the Reynolds number is shown in Figure 2. For Reynolds numbers $10^3 < Re < 10^4$, the Strouhal number remains fairly constant at 0.21. The Strouhal number is the established criteria for the determination of the periodicity of the wake for a certain flow velocity and cylinder diameter.

2.3 The Effects of a Nearby Plane Boundary on the Flow Around a Cylinder

2.31 Real Fluid Flow

When a cylinder is located close to a wall, the constriction of space between the cylinder and the wall causes the flow of water in that area to accelerate. Because of the fluid acceleration, the fluid in the cylinder boundary layer (near the plane boundary) will increase in velocity and gain momentum. Thus, the separation point on the cylinder surface near the plane boundary will move downstream.

R. Brown (1) concluded that a pipe on the bottom of a channel with fluid flowing perpendicular to its axis in the Reynolds number range of $1\text{-}3 \times 10^5$ exhibits properties of lift and drag similar to that of a wing on an airplane. It was also noted that the coefficient of drag with the pipe on the plane boundary was less than that of the pipe suspended with flow around both top and bottom.

In a paper written by J. J. Cornish III (3), it was mentioned that the situation where a cylinder is near a plane boundary is strongly affected by the boundary layers which may exist on the cylinder and on the wall. The lift forces acting on the cylinder were reported to be reduced because of these boundary layers. However, a positive lift force and an increase in the drag force was suggested to exist when the cylinder was near a boundary.

In a paper by J. Wilson and H. Caldwell (17), the affect of currents on pipes anchored above the ocean floor was studied. It was reported that for a cylinder nearing a plane boundary the coefficient

of drag was quite sensitive to the Reynolds number when a ground plane was present.

To the author's knowledge, no information is available on the subject of cylinder vortex formation and shedding near a plane boundary. However, in past experimental work, it has been noted by G. E. Mattingly (7) and F. Shair (15) that sidewall confinement of a cylinder might account for increased stability of the wake.

2.32 Complex Potential

From potential flow theory, near a plane boundary, uniform flow around a cylinder may be represented mathematically by flow around two cylinders as shown in Figure 3, (8). Both cylinders C1 and C2 can each be represented by a system of doublets. When the two systems are far apart, the doublet induced velocity flow from one will not appreciably affect the other. However, as the two systems move closer to each other or for a decreasing value of 2s/a, each doublet affects the other in the form of added velocity components. If a circle of radius a is scribed around the doublet with its center at the doublet center, the boundary condition on the circle demands that the sum of the normal velocity components be zero in order that the circle represent the flow boundary of a rigid cylinder. However, there are added velocity components on the circle due to the affects of the summetrically opposite doublet. To satisfy the boundary condition, these added velocity components can be negated by the distribution of doublets inside the circle (18). Milne-Thomson's circle theorem (8), can be used to find the location and strength of these

image doublets. Referring to Figure 4, the complex potential can be expressed as

$$W = Ua^2\left[\frac{1}{z} + \frac{1}{z-i2s} + \frac{a^2/4s^2}{z-i(2s-\frac{a^2}{2s})}\right] \qquad (4)$$

where U = free stream velocity

a = cylinder diameter

2s = distance between the center of the cylinders

$i = \sqrt{-1}$

From the complex potential, it can be seen that along with the original doublets of strength Ua^2 at z = i2s and z = 0, there is an additional smaller doublet of strength $Ua^2\ a^2/4s^2$ at $z = i(2s-(a^2/2s))$. This extra doublet m_1 at C1 negates the added velocity components due to the doublet m_0 at C2.

To keep the symmetry of the flow, a doublet with strength m_1 should be located in circle C2. Each of these added smaller doublets introduce yet other velocity components on the opposite cylinders. Many smaller doublets must continually be introduced to counteract the induced flow created by the preceding doublet. Converging to the radius of the cylinder the doublets can be expressed (18) as the infinite series

$$W = Uz + Ua^2q_1^2q_2^2\cdots q_n^2\left(\frac{1}{z-i(s-aq_n)} + \frac{1}{z+i(s-aq_n)} + \cdots\right) \qquad (5)$$

where

$$q_n = 1/\{(2s/a) - q_{n-1}\}, \; q_o = 0$$

A computer program, courtesy of T. Yamamoto, was utilized to numerically compute the complex potential using the technique just described and it can be found in Appendix 10.

2.33 Front Stagnation Point of the Cylinder Surface

The stagnation point on the cylinder surface can be found by determining the position where the tangential doublet induced surface velocity is zero. The technique employed to find the stagnation point was developed by T. Yamamoto and the computer program created for this purpose may be found in Appendix 10.

2.34 Separation Point of the Cylinder Boundary Layer for Laminar Boundary Layers

An approximate method due to T. von Karman and K. Pohlhausen, (2) and (14), for two dimensional flows was used in this thesis to find the separation point for the laminar boundary layer conditions. This method essentially involves using the momentum equation

$$U^2 \frac{d\delta_2}{dx} + (2\delta_2 + \delta_1) U\frac{dU}{dx} = \frac{\tau_o}{\rho} \qquad (6)$$

where δ_1 = displacement thickness

δ_2 = momentum thickness

U = velocity

τ_o = shear stress

as an ordinary differential equation for the boundary layer thickness. The separation point can be found by locating the position where the shear stress goes to zero. In using this method, the existance of a no-slip condition at the cylinder surface is used. The fluid velocity and velocity gradient along the cylinder surface was found by the technique described in section 2.32 and 2.33 based on potential flow theory. After the pressure distribution around the cylinder was obtained, the separation points of the cylinder boundary layer were found using equation (6). The computer program shown in Appendix 10 was utilized to compute the separation points of the cylinder boundary layer.

The von Karman and Pohlhausen approximation may have severe limitations if it is to be applied to the entire flow configuration around a circular cylinder. Referring to Figure 5-A, the two separate ideal real fluid flow regimes are divided by a streamline and the cylinder boundaries. These boundaries separate the flow into symmetrically, independent similar zones. In Figure 5-B, the streamline around the cylinder which was marked as the dividing boundary between the two flow regimes is characteristic of a cylinder that is nearing a wall for ideal fluid flow. As the reader will notice, the upper zone is not symmetrical to the lower zone.

In Figure 5-A, the pressures along the upper zone cylinder boundary H will be identical to the pressures along the lower zone cylinder boundary L, due to the symmetry of the two regions. However, as is shown in Figure 5-B, these two regions are not symmetrical due

to the proximity of a nearby plane boundary. Because there exists relative independence of flow characteristics between the two zones and these zones are unsymmetrical, the pressures along each of the cylinder boundaries T and B will be unsymmetrical and the pressures at the separation points along the cylinder surface may be different. For example, for an e/D=0.0125, the non-dimensional pressure at the upper separation point was predicted to be -3.1 while the lower separation point was predicted to have a pressure of -7.2 by this approximation method.

Physically, in real fluid flow around a cylinder near a plane boundary, these conditions can never exist and to assume such a condition will lead to error in the calculation of the separation point on the cylinder boundary layer. For, in under real flow conditions, the pressure in the wake of the cylinder is approximately equal near both of the separation points of the cylinder boundary layer.

2.35 Force on the Cylinder

In order to calculate the force on the cylinder as it nears a plane boundary, the complex potential as found in section 2.32 is used for potential flow. The total force on the cylinder being considered can be expressed as the sum of the many doublet-doublet interactions existing in the system shown in Figure 4,(18).

Using the theorem of Blasius, after integrating the complex potential found in section 2.32 around the cylinder, the horizontal and vertical force is found to be

$$F_H = 0$$

$$F_V = -4\pi\rho \sum_{j=0}^{\infty} \sum_{k=0}^{\infty} \frac{m_j m_k}{(2s - a(q_j + q_k))^3} \qquad (7)$$

where q_j or $q_k = 1/((2s/a) - q_h - 1) \quad q_o = 0$

Usually a coefficient of lift and drag is found to be a more common way of expressing the vertical and horizontal force on the cylinder, respectively. The lift and drag coefficient is defined as

$$C_L = F_V/\tfrac{1}{2}\rho U^2 D \qquad (8)$$

$$C_D = F_H/\tfrac{1}{2}\rho U^2 D \qquad (9)$$

where D = cylinder diameter

U = stream velocity

3.0 EXPERIMENTAL TECHNIQUE AND EQUIPMENT

3.1 Laboratory Equipment

An eight foot long channel with a self-enclosed circulation system containing twenty-one cubic feet of water was used as the setting for the experimentation for this thesis. As shown in Figure 6, the channel itself was made of ½" plexiglass and was four inches wide by two feet high. The head tank was joined to the channel by a specially designed nozzel as shown in Figure 7.

3.2 Force Measurement Technique

Before the experiment was actually conducted, the flow in the channel was adjusted so that it was uniform, to within five per cent of the average mainstream velocity. A vertical and horizontal velocity profile was taken using a pitot tube and pressure transducer. Results can be found in Figure 8 and 9. The boundary layer along the bottom of the channel was less than a sixteenth of an inch at the positions where data was obtained.

The cylinder strain-gauge system used for measuring the forces on the cylinder is shown in Figure 10. Each cylinder was rigidly connected to a ¼" aluminum bar which was strain-gauged. This system was in turn connected rigidly to a carriage device which was able to move both vertically and horizontally along the channel. For each experimental run the carriage was fixed horizontally 1.5 feet from the channel entrance and the cylinder was moved vertically to obtain a force profile. At all times, the ends of the cylinder were

approximately a sixteenth of an inch from the cylinder. The total cylinder system was rigid enough to limit cylinder oscillations to less than 0.05 cylinder diameters but sensitive enough to permit strain-gauge readings of one gram of force. The force measuring system was arranged so that drag and lift could be measured separately. Due to the inherent physical characteristics of the force measuring equipment, no readings could be taken when the cylinder touched the wall.

3.3 Flow Visualization Technique

In order to physically locate the separation point and stagnation point of the boundary layers, the tiny air bubbles that were inherent to the channel system and that completely saturated the flow were used. Both points showed clearly in the photographs taken of the flow around the cylinder.

4.0 RESULTS

4.1 Drag on the Test Cylinder

The coefficients of drag for the test cylinder are plotted against e/D in Figure 11 for subcritical Reynolds numbers. For all tests conducted, there existed a definite increase of approximately 13% in the coefficient of drag as the cylinder got within approximately 1.5-2.0 cylinder diameters from the plane boundary.

When the test cylinder was more than two cylinder diameters from the plane boundary, coefficients of drag between 1.0 and 1.4 were recorded.

Due to the physical limitation of the force measuring system, the coefficient of drag could not be measured when the cylinder touched the plane boundary.

It is the opinion of the writer that the scatter evident in the data taken at the lower Reynolds number is due to operating in the range of the instrument limitations. Because the force was small at the slower water velocities, the signal to noise ratio became small and mechanically the force measuring device was approaching its limitations.

4.2 Lift on the Test Cylinder

Coefficient of lift data is plotted against e/D in Figures 12-14 for subcritical Reynolds numbers. For all test runs completed, there was a definite positive lift force that started when the

cylinder got within approximately 1.8 cylinder diameters away from the wall, increasing as the cylinder got closer to the plane boundary.

Again, the scatter that exists for the data taken at the lower Reynolds numbers can be explained as due to the signal to noise ratio being small and mechanically the force measuring device approaching its limitations.

4.3 Stagnation and Separation Points of the Cylinder Boundary Layer

Referring to Figure 15, as the cylinder neared the plane boundary, there was a tendency for the front stagnation point of the cylinder boundary layer to move downward. Data obtained from potential flow theory was in good agreement with the experimental data.

As can be seen in Figure 16, as the cylinder nears a plane boundary, there is a tendency for the upper separation point of the cylinder boundary layer to move forward while the lower point of separation moves toward the rear of the cylinder. Data from the von Karman and Pohlhausen approximation method was not in good agreement with the experimental data. As is explained in section 2.34, this conflict was predictable.

4.4 Separation Point of the Channel Bottom Boundary Layer Near the Test Cylinder

For a certain Reynolds number, the position of the bottom wall boundary layer separation point was found to vary a function of e/D. As the test cylinder moved closer to the channel bottom, this

separation point moved closer to the test cylinder from a downstream position as is shown in Figure 17.

5.0 DISCUSSION

It was found that the drag increases as a cylinder nears a plane boundary. Comparisons are made with past experimental results as shown in Figure 18.

In reference (3) there was a suggestion that the coefficient of drag does increase as a cylinder neared a plane boundary, although no experimental data is shown to substantiate this view. References (1) and (17) showed data that does not agree with the author's.

To the writer's knowledge, no other past experimental results in the subcritical Reynolds number range were known to exist.

The apparent increase of drag as the test cylinder neared the plane boundary was substantiated by an observed increase in the wake area. It is the writer's opinion that the wake was stabilized, as was observed experimentally, and thus the wake turbulence decreased. With a decrease in wake turbulence, the vortices shed by the cylinder were not dissipated as quickly as before, thus helping to extend the wake area. The drag on a body is directly related to wake geometry and thus, if the wake area is increased, the drag on that body is increased.

Comparisons were made with past experimental and theoretical values of the coefficient of lift as shown in Figure 19. Potential flow theory can be seen to predict a negative lift force until the cylinder touches the wall, where it becomes positive. From the assumptions of the potential flow theory which were discussed in section 2.2, one may make conclusions as to why the predictions of

this theory differ so drastically from the experimental values. Potential flow theory requires irrotational flow particles in the regime in which the theory is to be used. Clearly, in real flow, a large portion of the flow regime around a cylinder consists of rotational flow, such as the wake and cylinder boundary layer. Large error will then result from using potential flow theory as was indicated by the experimental data.

Data from references (3), (4) and (17) indicate a positive lift force when the cylinder is near a plane boundary. The author was not able to verify the validity of the data from reference (4) because a published copy of the experimental work could not be obtained.

When a cylinder is located close to a wall, the constriction of space between the cylinder and the wall causes the flow of water in that area to accelerate. Because of the fluid acceleration, the fluid in the cylinder boundary layer near the plane boundary will increase in velocity and gain momentum. This added momentum would allow the fluid in the cylinder boundary layer to travel further along the cylinder surface before separation of the boundary layer would occur. If the bottom separation point does move downstream, as was indicated by experimental data in Figure 16, then the wake will have a tendency to form at an angle going away from the plane boundary, as can be seen in the pictures in Figures 17 and 20. As the front stagnation point moves downward, as shown in Figure 15, the angle of the axis of the wake perpendicular to the cylinder axis will be going away from the plane boundary as is shown in Figure 17

and 20.

The wake may have an inclination to maintain its symmetrical nature and thus the top separation point will move forward along the cylinder surface, as is indicated by experimental data in Figure 16. The mainstream fluid particles, traveling much faster than those in the wake, will have a tendency to mold the wake into the geometry that existed when the cylinder was far away from the plane boundary. It was observed during the experiment that the fluid particles at the rear of the wake several cylinder diameters downstream were traveling horizontal to the plane boundary again. The tendency then, is for the fluid particles in the wake to form an aerofoil configuration as they move around the cylinder. Thus, a low pressure area will exist in the top portion of the cylinder wake, creating lift.

Experimental data did indicate that there was separation of the channel bottom boundary layer behind the cylinder for $0<e/D<0.4$. This separation as shown in Figure 17 would definitely have the effect of pushing the wake vertically upwards helping to create an aerofoil wake configuration. As the cylinder got nearer to the plane boundary, the separation point moved closer to the cylinder. Thus, this separated boundary layer would have an increasing significant effect on the lift of the cylinder as it got closer to the plane boundary.

6.0 CONCLUSIONS

1. The coefficient of drag increases approximately 13% from a point approximately 1.5-2.0 cylinder diameters away from the wall, remaining fairly constant to the plane boundary.

2. The coefficient of lift increases in a positive sense from a point approximately 1.8 cylinder diameters away from the wall, increasing in value as the cylinder nears the plane boundary. Experimental data negated potential flow theory results.

3. The cylinder exhibits the geometric form and properties of an aerofoil near a plane boundary.

4. The front stagnation point of the cylinder boundary layer moves downward, following the predictions of potential flow theory, near a plane boundary.

5. The upper separation point of the cylinder boundary layer moves toward the front of the cylinder while the lower separation point moves toward the rear of the cylinder as a cylinder nears a boundary. Results from the von Karman and Pohlhausen approximation did not match experimental data.

6. Separation of the channel bottom boundary layer occurs downstream of the cylinder; the point of separation moving closer to the cylinder as it is moved closer to the plane boundary.

7.0 LIST OF REFERENCES

1. Brown, R. J. Hydrodynamic Forces on a Submarine Pipeline. Journal of the Pipeline Division, American Society of Civil Engineers. Vol. 93, no. PLI, March 1967.

2. Chang, P. K. Separation of Flow. Pergamon Press, 1970.

3. Cornish III, J. J. Some Aerodynamic Characteristics of Land Vehicles AIAA Symposium of Aerodynamics of Sports and Competition Automobiles. Los Angeles, April 1968.

4. Ippen, A. T. Estuary and Coastline Hydrodynamics. McGraw-Hill Book Co., Inc., pp. 375, 1966.

5. Karman, Th. von and H. Ruback. Uber den Mechanismus des Flussigkeits und Luftwider-standes. Phys. Z. 13, pp. 49-59, 1912.

6. Marris, M. V. A Review on Vortex Streets, Periodic Wakes, and Induced Vibration Phenomena. Journal of Basic Engineering. Transactions of the American Society of Mechanical Engineers, June 1964.

7. Mattingly, G. E. An Experimental Study of the Three-Dimensionality of the Flow Around a Circular Cylinder. Institute for Fluid Dynamics and Applied Mathematics. University of Maryland Tech. Note BN-295, 1962.

8. Milne-Thomson, L. M. Theoretical Hydrodynamics. 5th edition. Macmillan, New York, 1968.

9. Morkovin, M. V. Flow Around Circular Cylinders - A Kaleidoscope of Challenging Fluid Phenomena. The Martin Co., Baltimore, Maryland.

10. Richter, Andreas. Stromungskrafte Auf Starre Kreiszylinder Zwischen Parallelen Wander. Doctoral Thesis, Institute fur Hydromechanik Universitat Karlsruhe, 1973.

11. Roshko, A. On the Wake and Drag of Bluff Bodies. Journal of Aerospace Sciences, Vol. dd, no. 2, 1955.

12. Roshko, A. On the Development of Turbulent Wakes from Vortex Streets. NACA Report 1191, 154.

13. Rouse, H. (Editor). Engineering Hydraulics. John Wiley and Sons, Inc., N.Y., 1950.

14. Schlicting, H. Boundary Layer Theory. McGraw-Hill Book Co., Inc., New York, 1968.

15. Shair, F. H., A. S. Grove, E. E. Petersen, and A. Acrivos. The Effect of Confining Walls on the Stability of the Steady Wake Behind a Circular Cylinder. Journal of Fluid Mechanics, Vol. 17, 1963, pp. 546.

16. Strouhal, V. Ann. Physik Chemistry. Vol. 5, 1878, pp. 216-251.

17. Wilson, J. F. and H. M. Caldwell. Force and Stability Measurements on Models of Submerged Pipelines. Preprints, Offshore Technology Conference, Paper no. OTC-1224, Houston, Texas, April 1970.

18. Yamamoto, T., J. Nath, and L. Slotta. Yet Another Report on Cylinder Drag or Wave Forces on Horizontal Submerged Cylinders. Bulletin no. 47, Engineering Experiment Station, Oregon State University, April 1973.

8.0 FIGURES

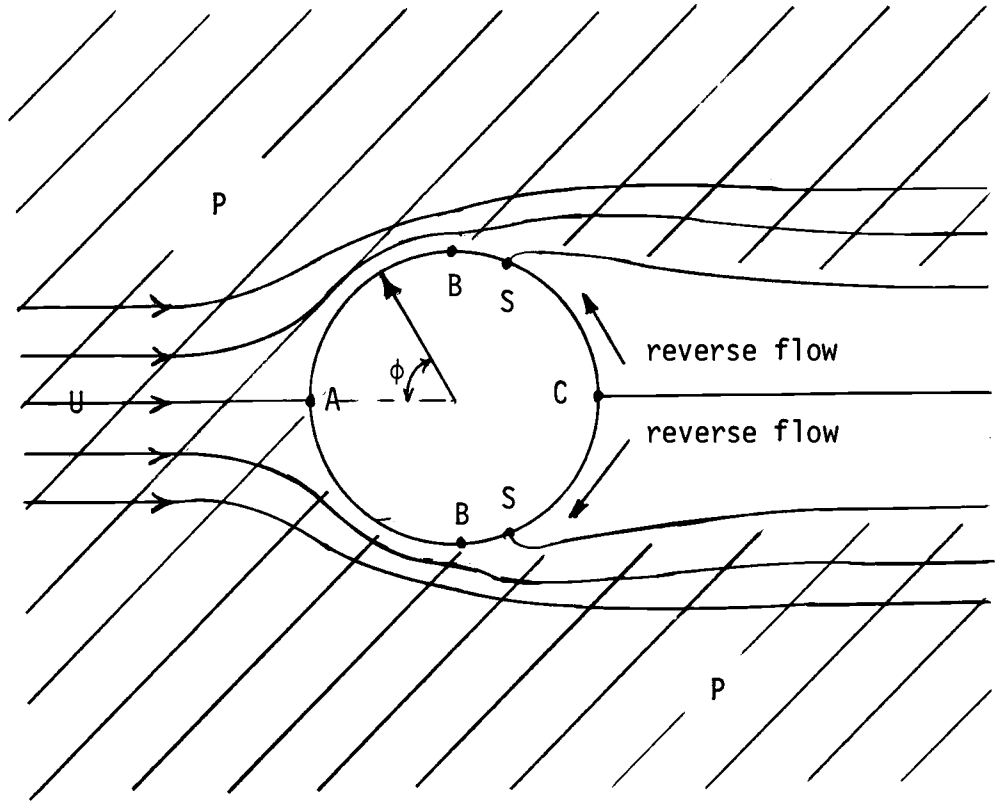

S = Points of separation

P = Region where the general flow displays irrotational characteristics

Figure 1 - Flow around a circular cylinder

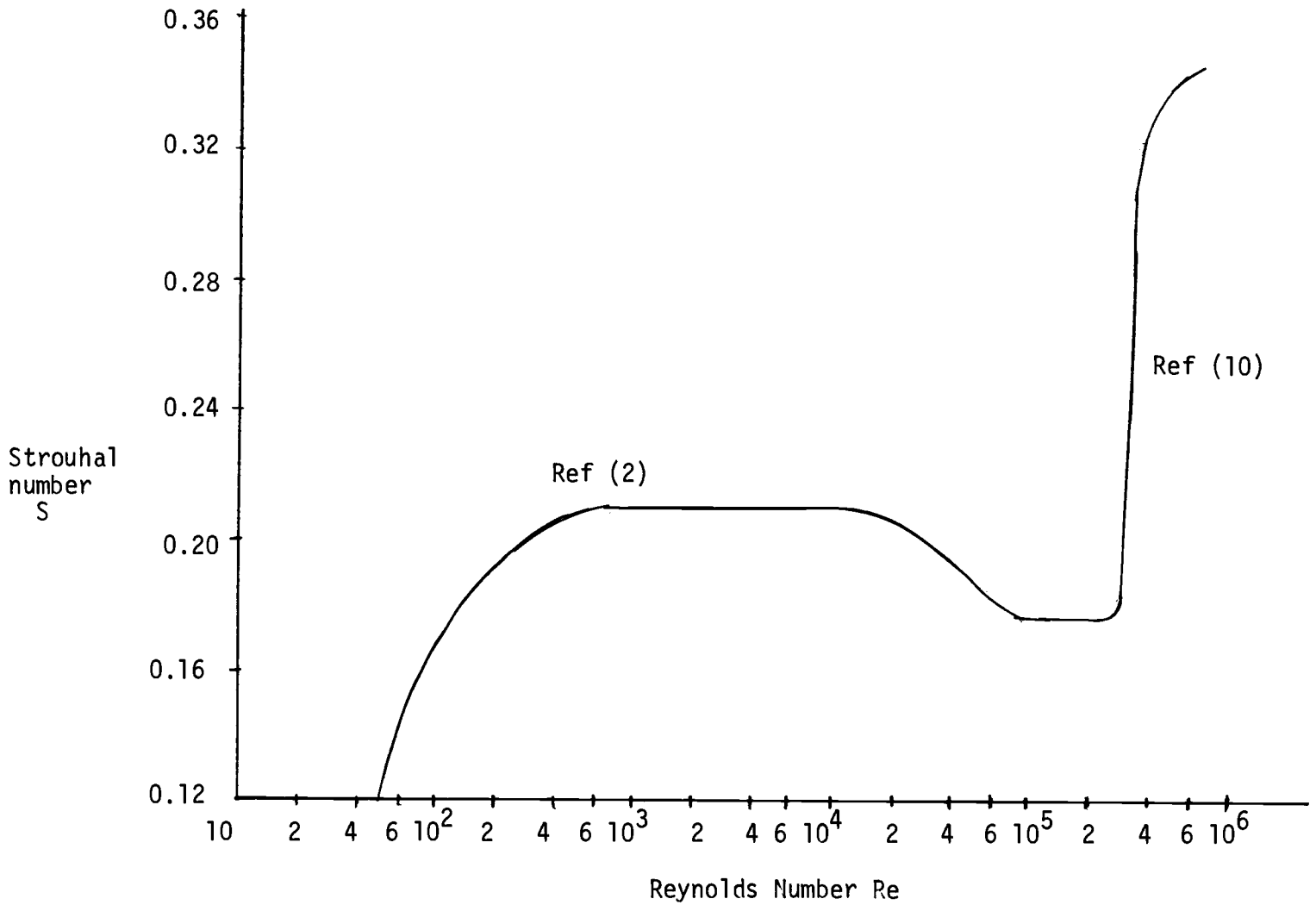

Figure 2 - Relationship between the Reynolds number and the Strouhal number

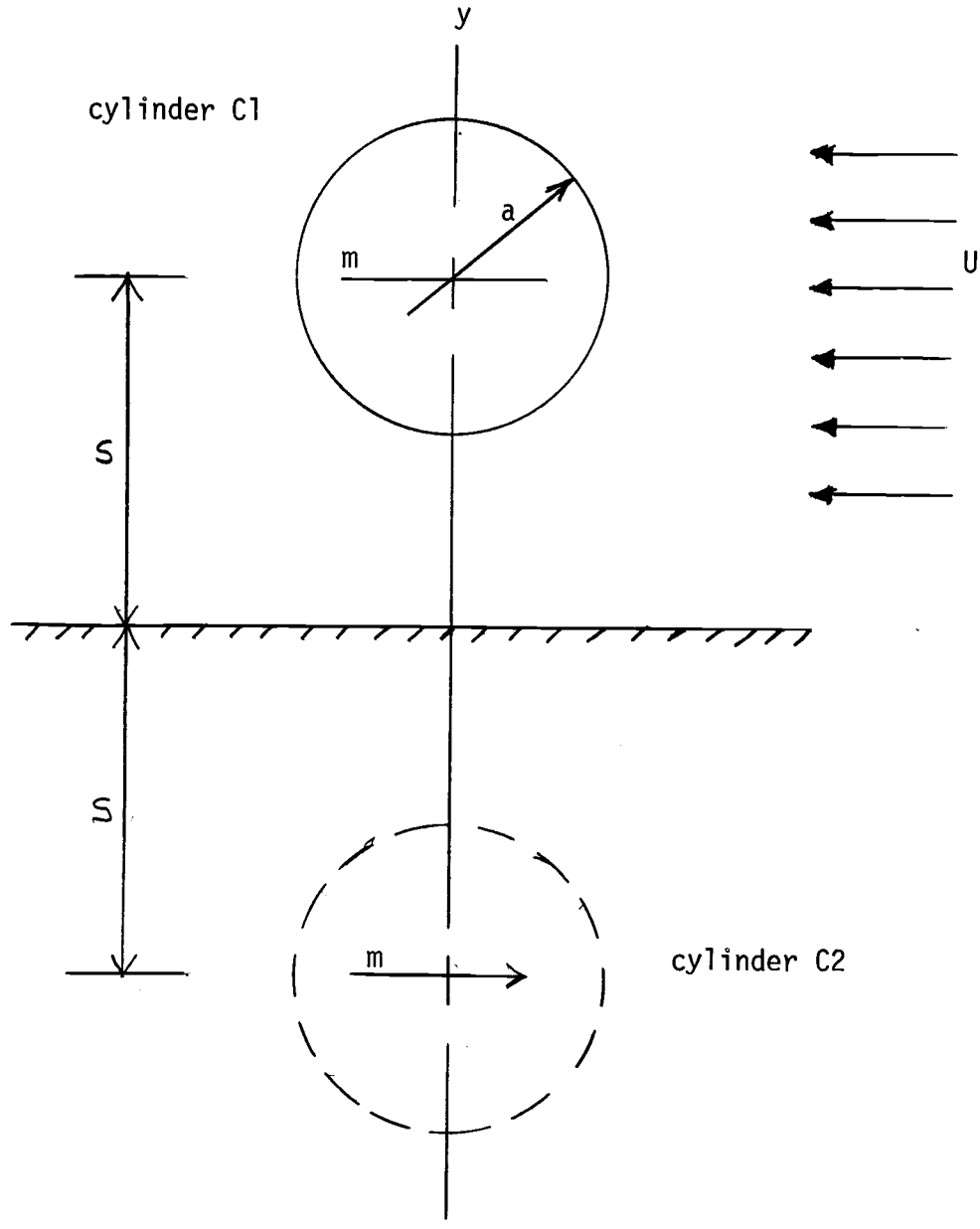

Figure 3 - Circular cylinder near
a plane boundary

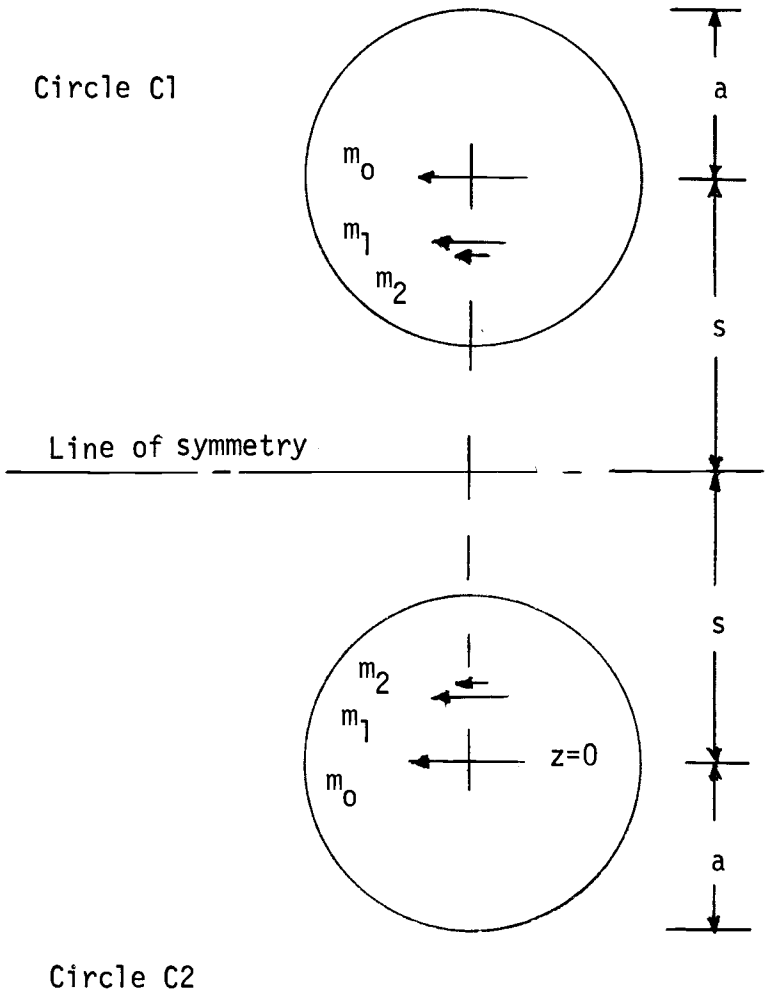

	Strength	Distance from center
m_o	Ua^2	0
m_1	$Ua\frac{2a^2}{4s^2}$	$\frac{a^2}{2s}$
m_2	$Ua\frac{2a^2}{4s^2}\frac{a^2}{(2s-\frac{a^2}{s})^2}$	$\frac{a^2}{2s-\frac{a^2}{2s}}$

Figure 4 - Distribution of doublets for uniform flow past two cylinders

A - Infinite stream

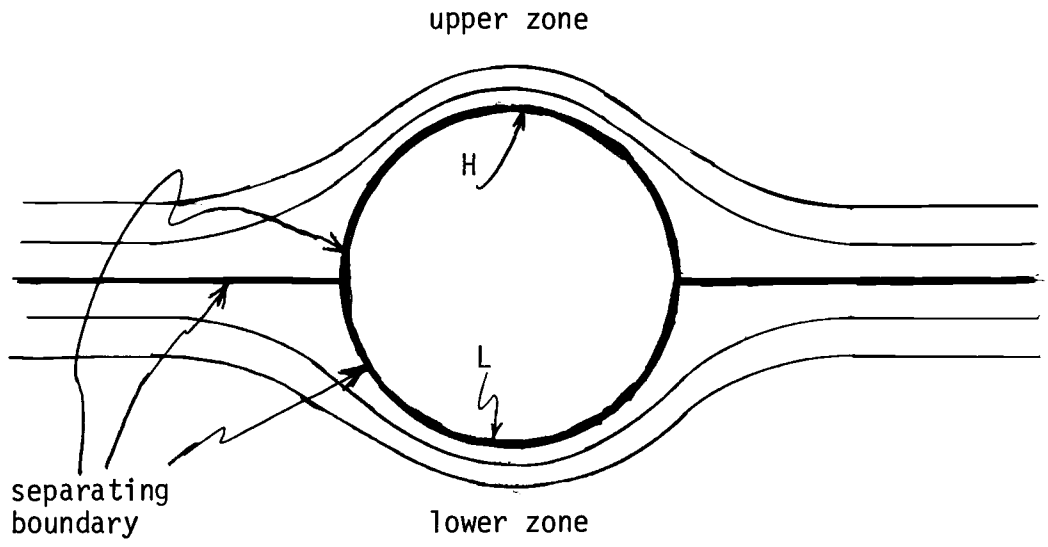

B - Near a plane boundary

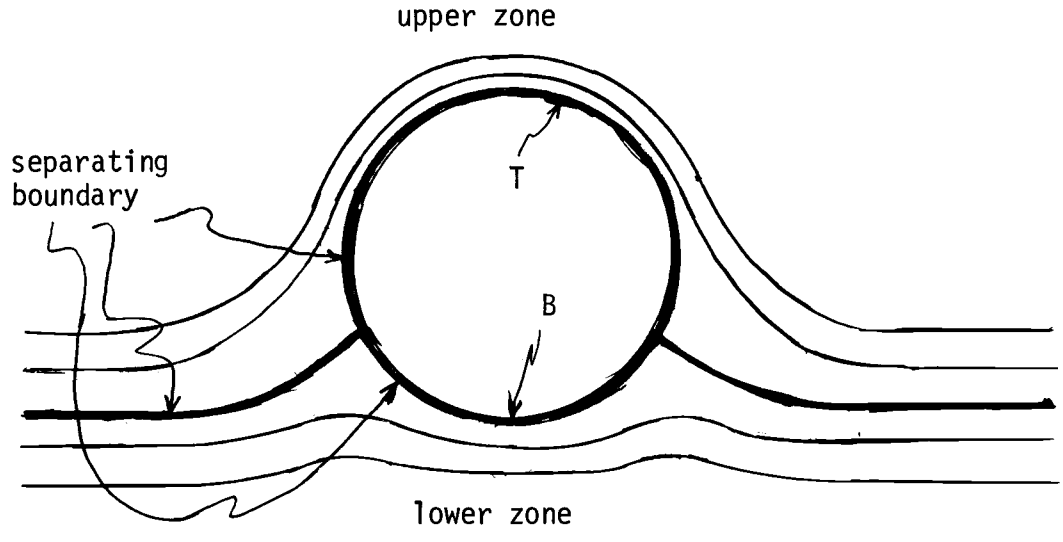

Figure 5 - Comparisons of streamlines around a circular cylinder near a plane boundary and in an infinite stream

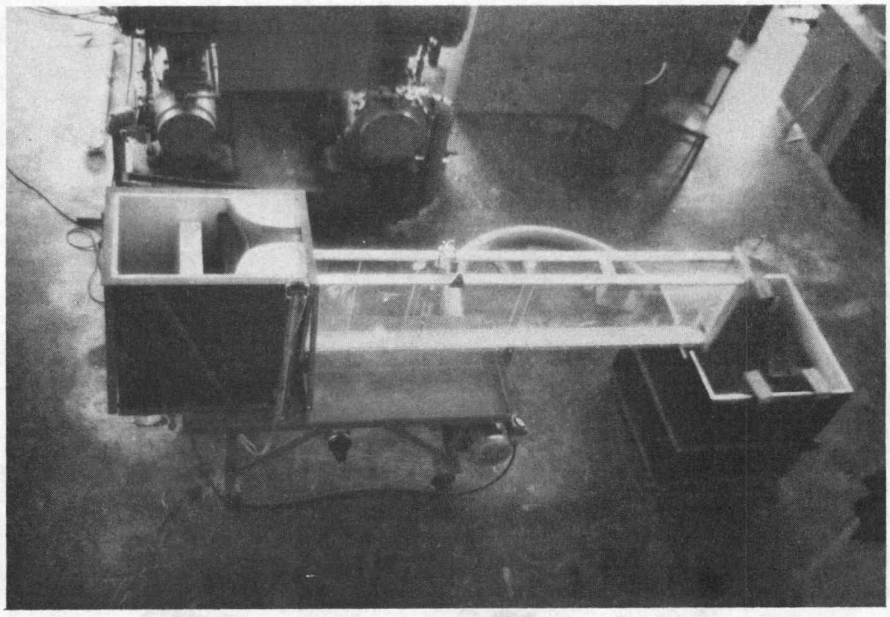

Figure 6 - Experimental apparatus

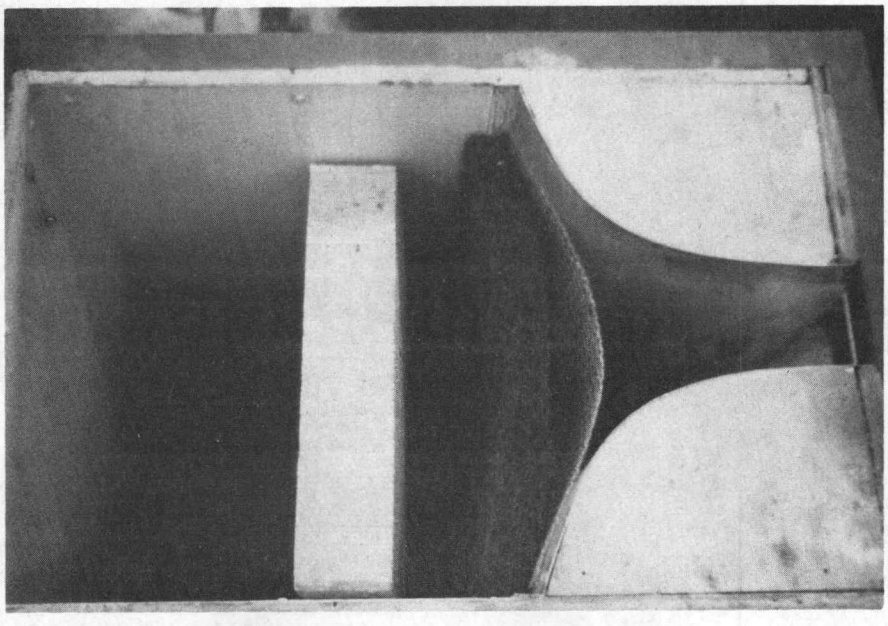

Figure 7 - Head tank

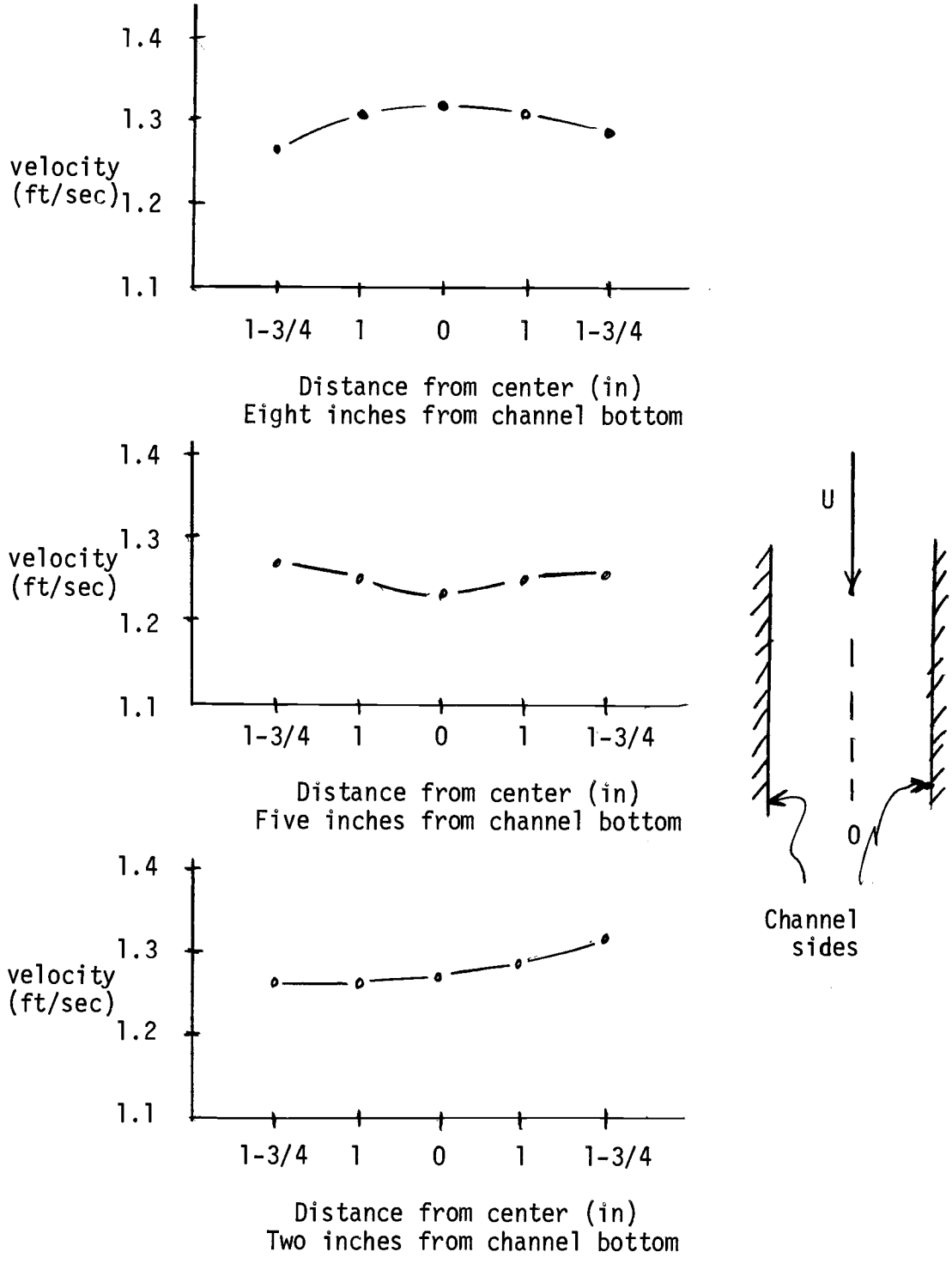

Figure 8 - Channel horizontal velocity profiles for uniform flow

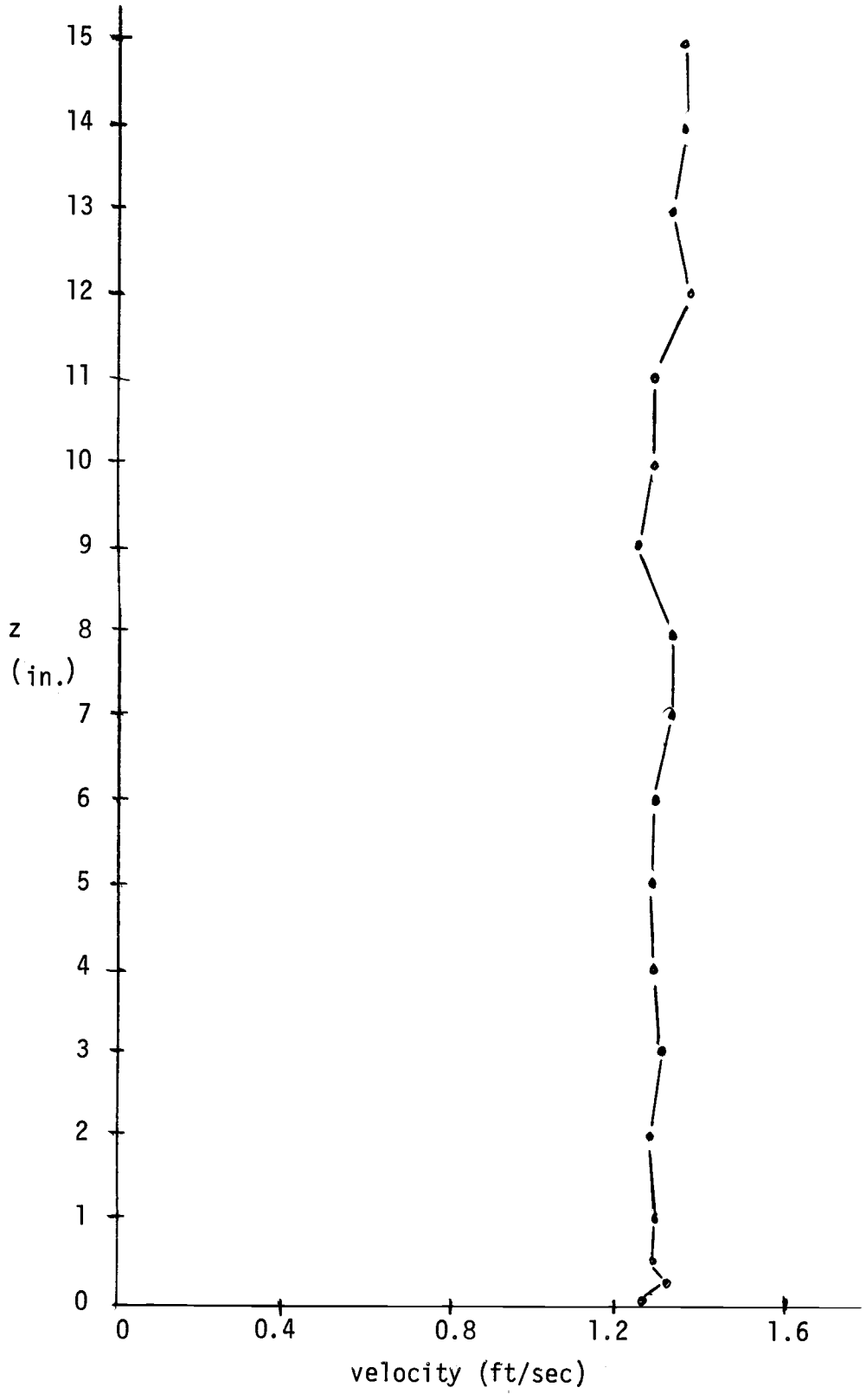

Figure 9 - Vertical velocity profile for uniform flow in the channel

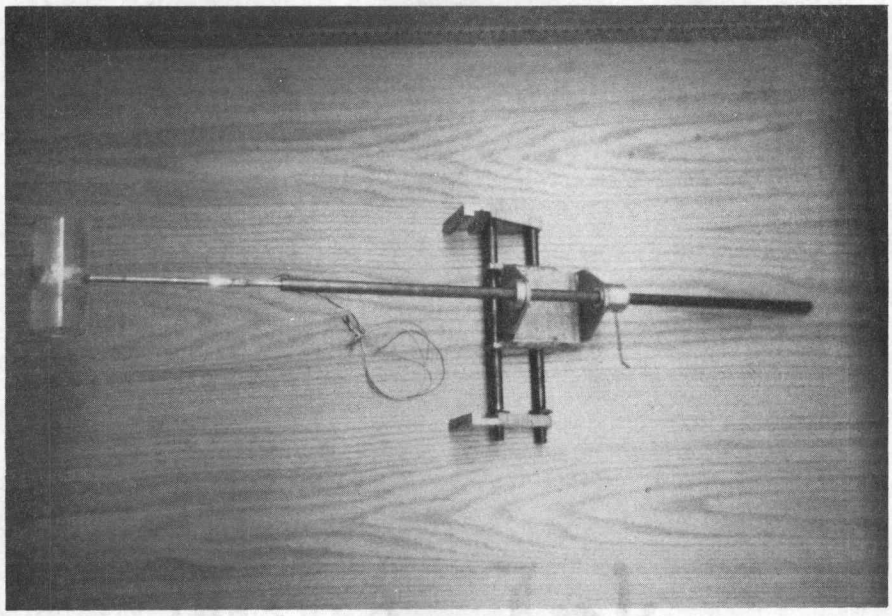

carriage and force measuring system

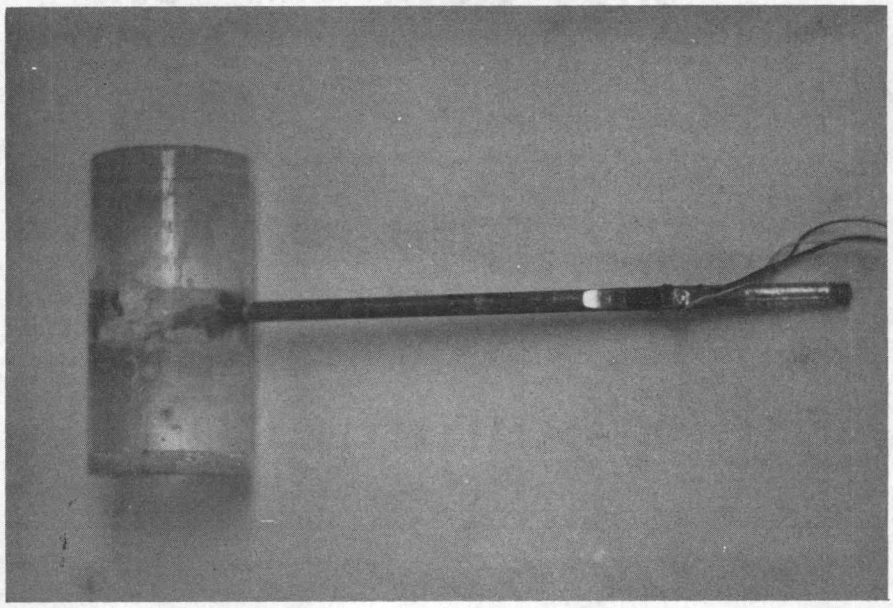

cylinder force measuring system

Figure 10 - Test cylinder and force measuring apparatus

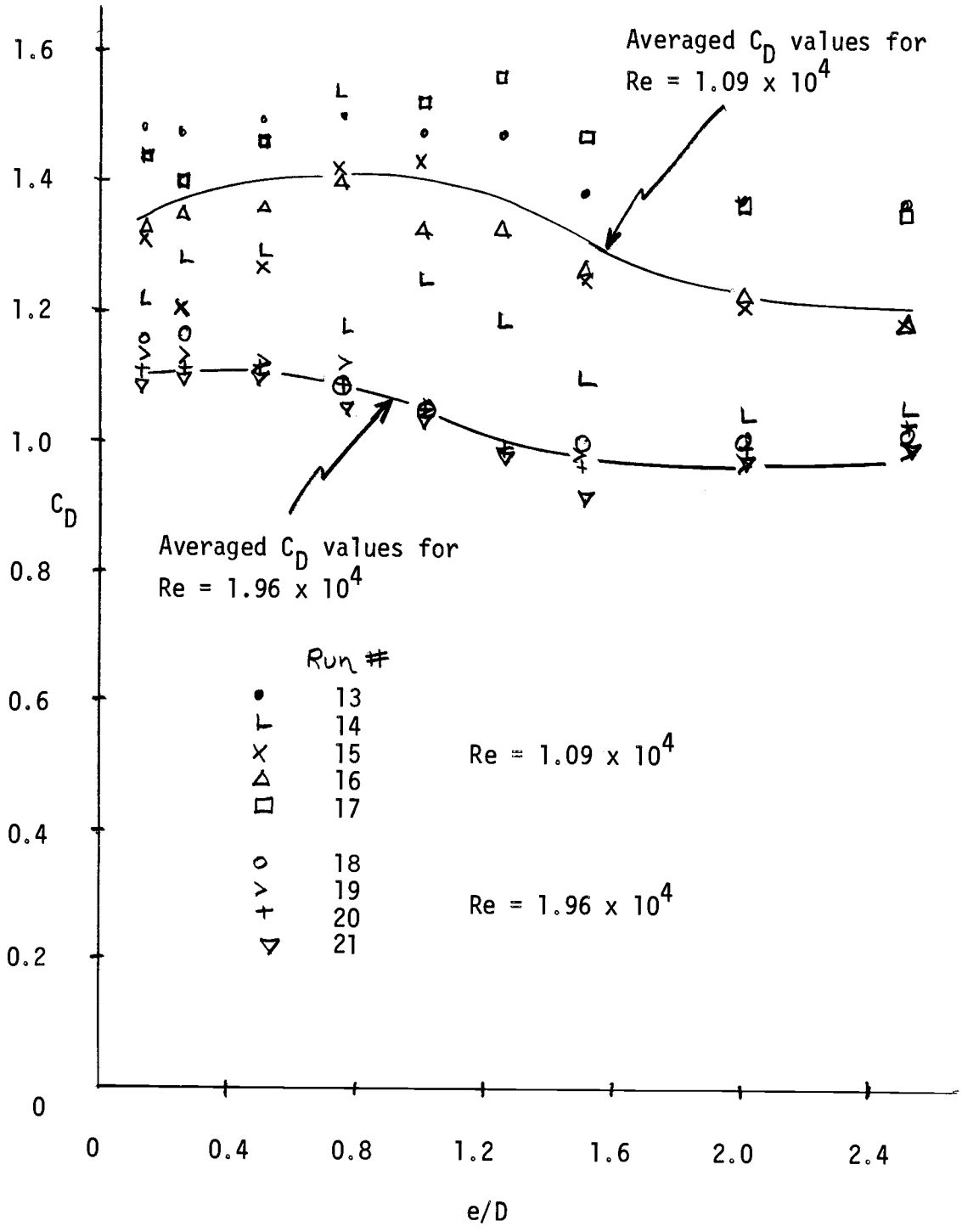

Figure 11 - Coefficient of drag plotted against e/D

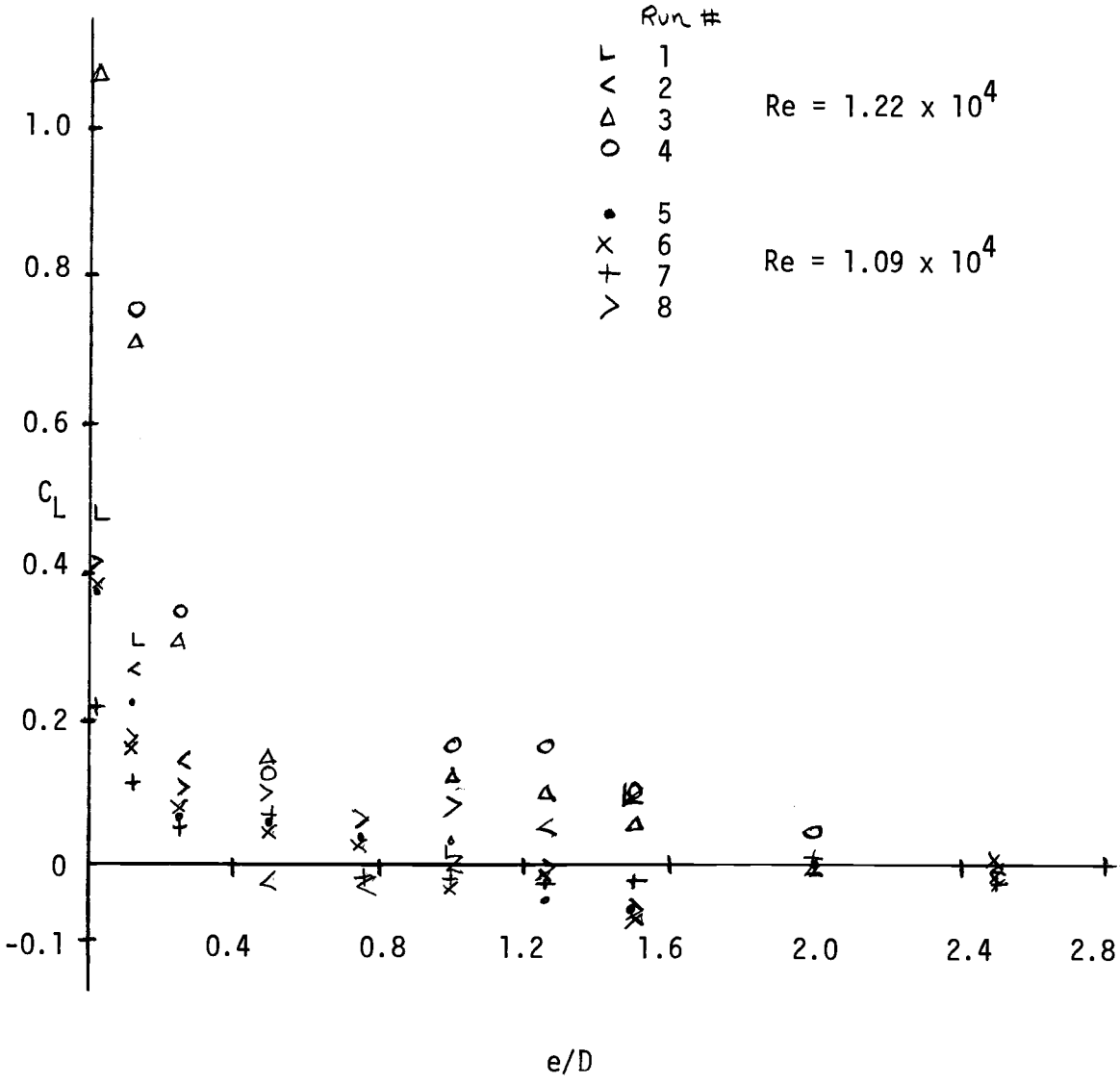

Figure 12 - Coefficient of lift plotted against e/D

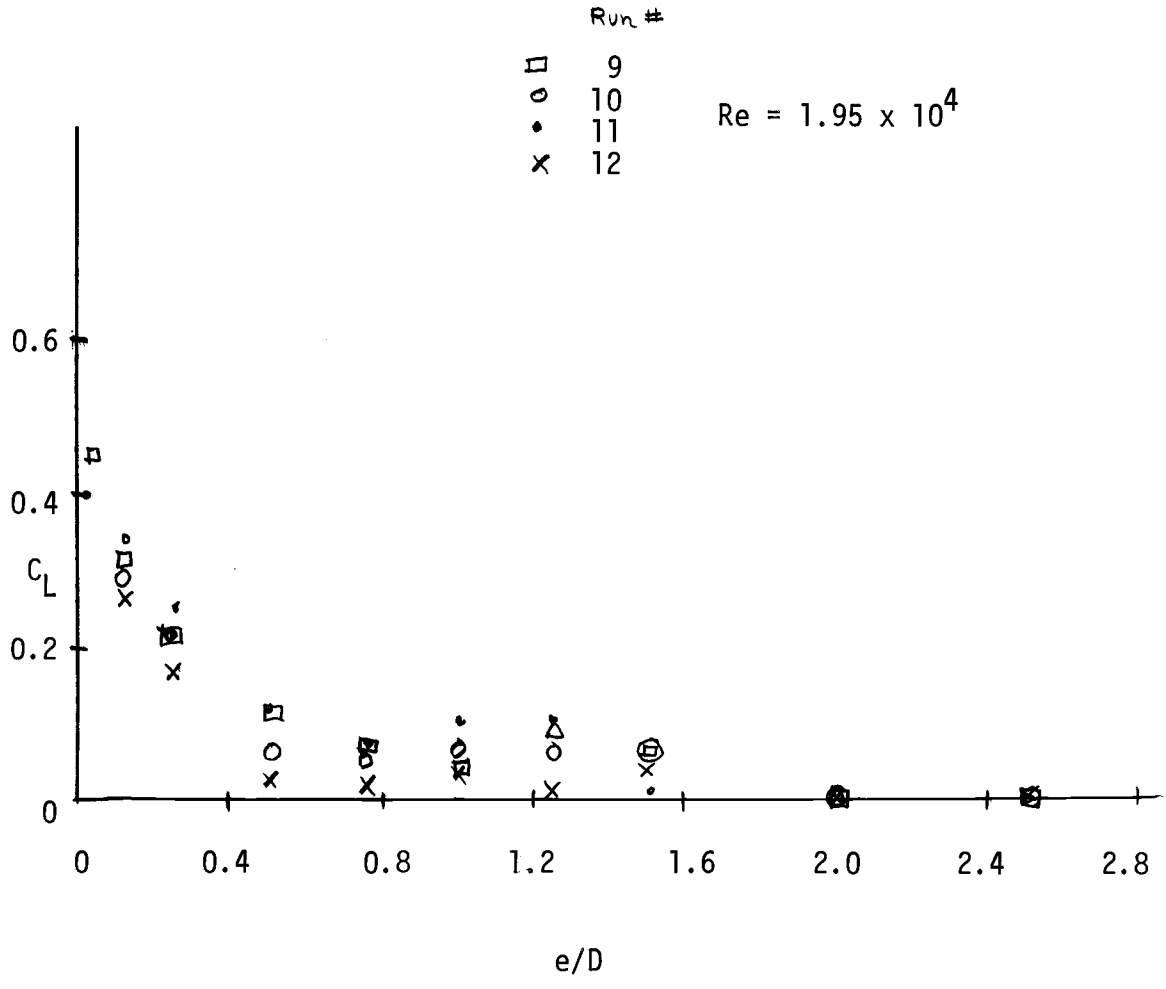

Figure 13 - Coefficient of lift plotted against e/D

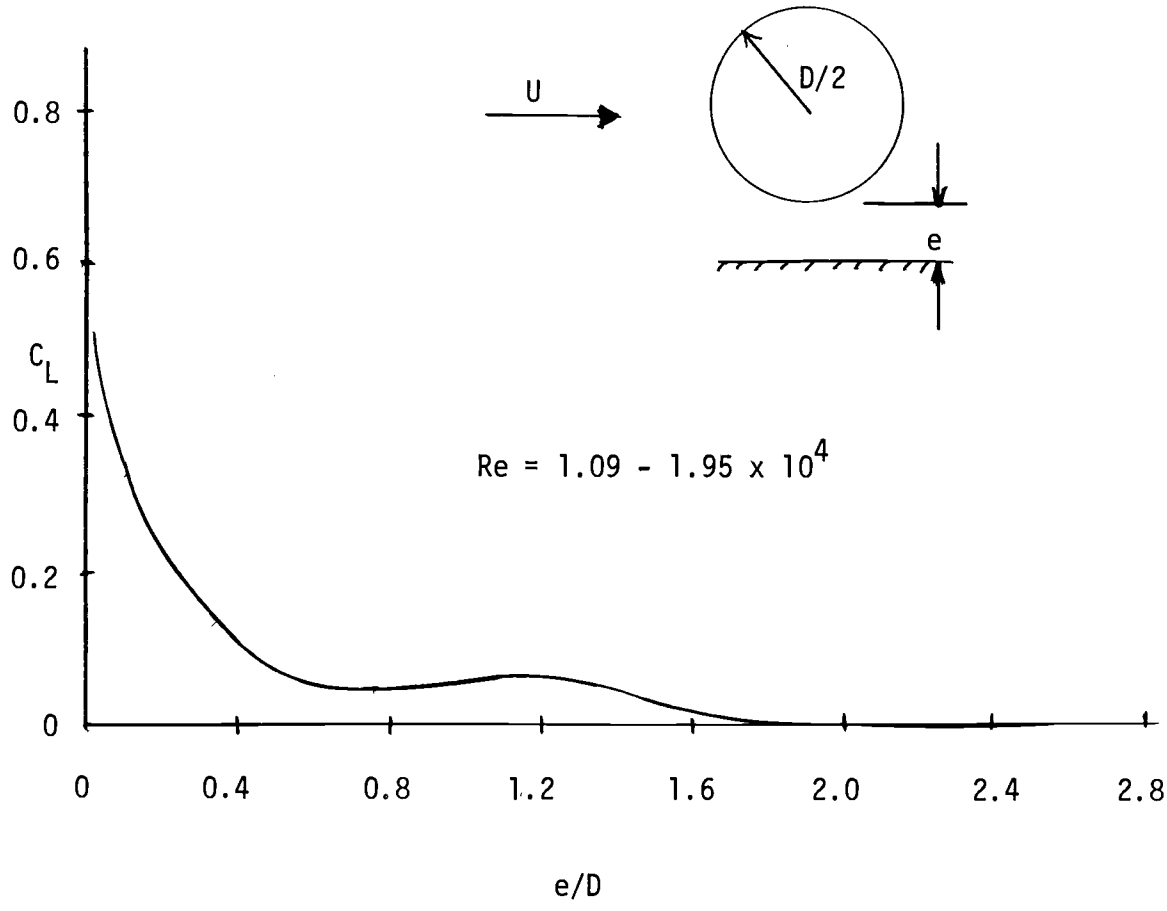

Figure 14 - Averaged values of coefficient of lift plotted against e/D

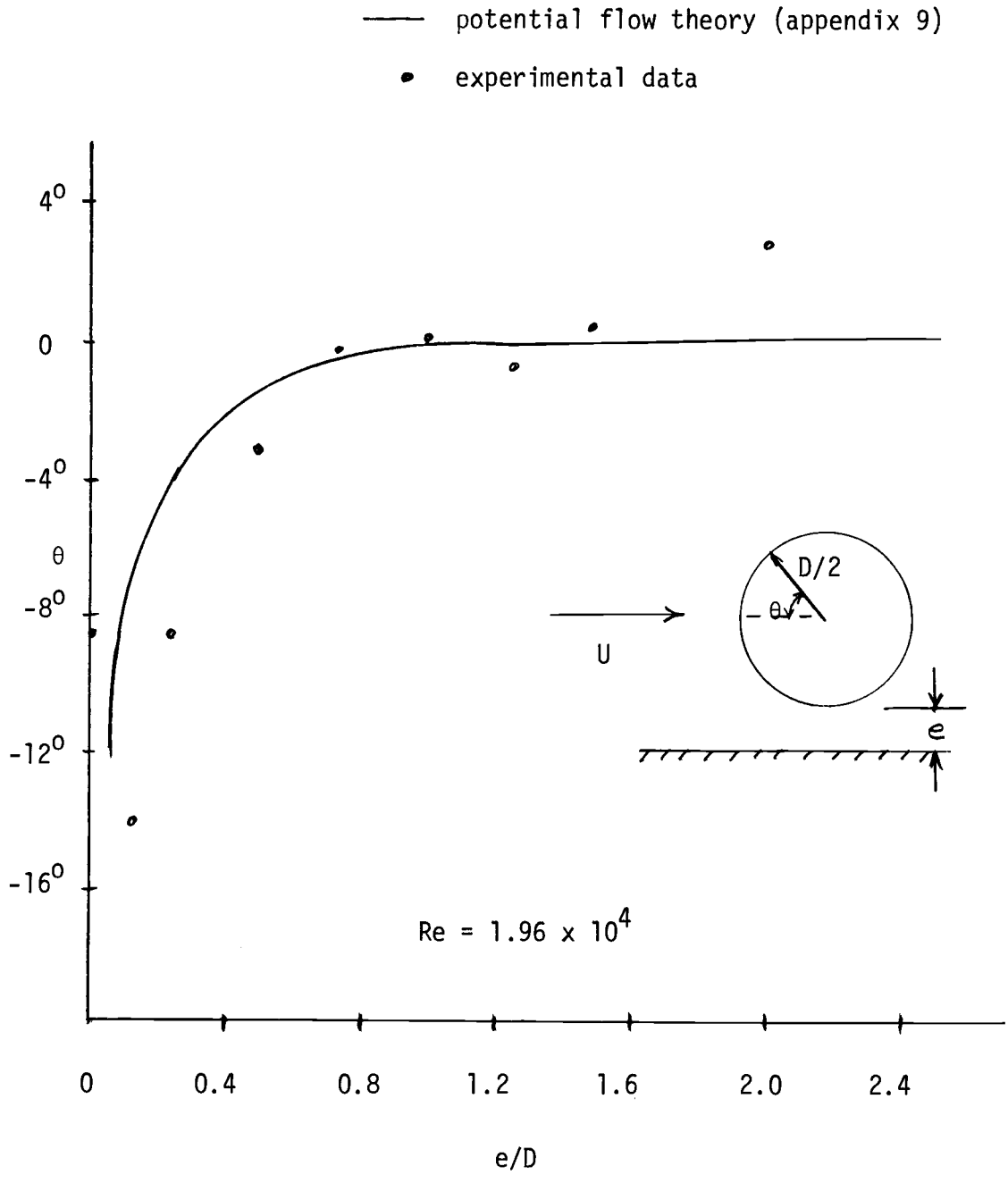

Figure 15 - Cylinder boundary layer stagnation point plotted against e/D

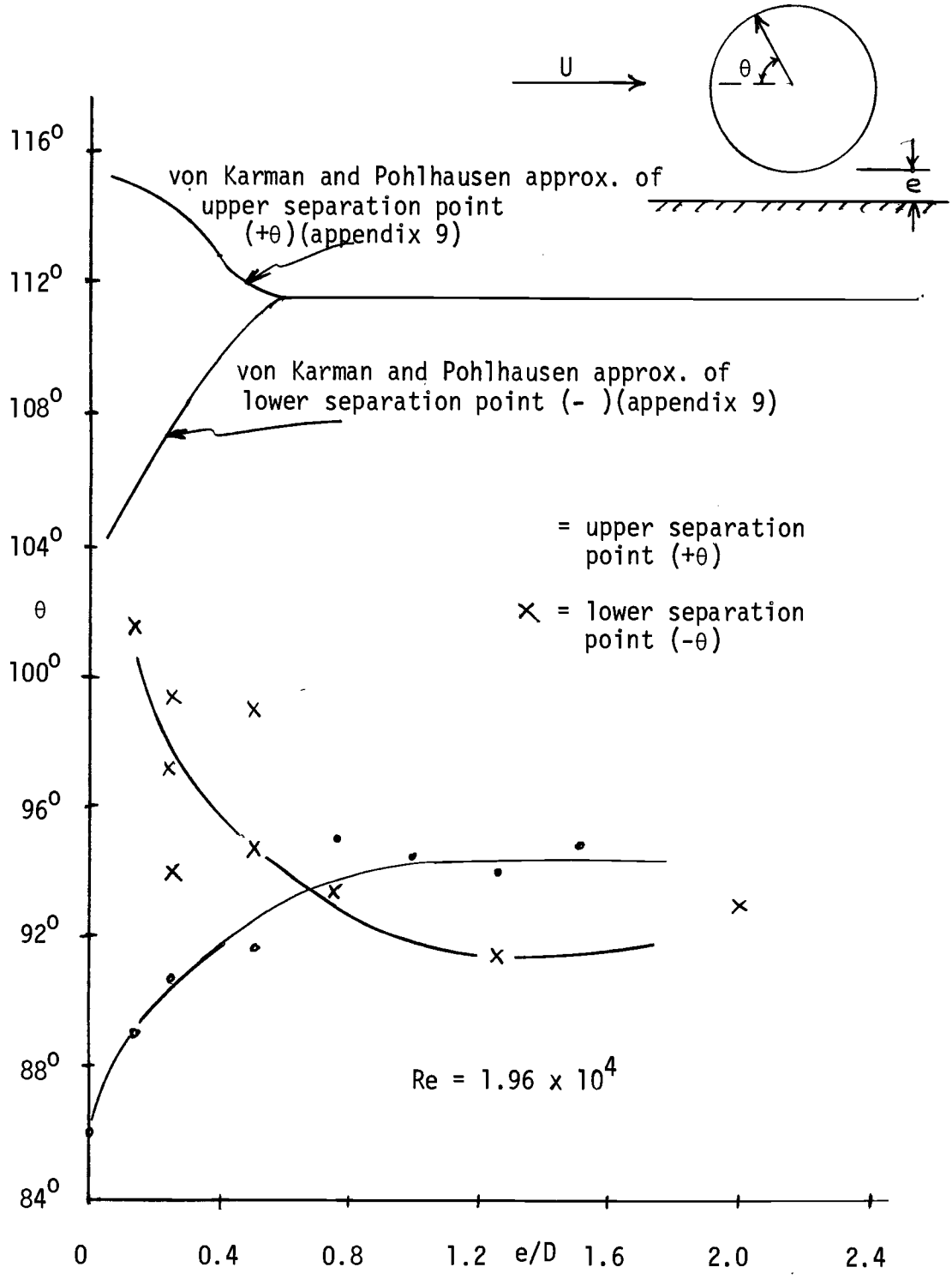

Figure 16 - Cylinder boundary layer separation points plotted against e/D

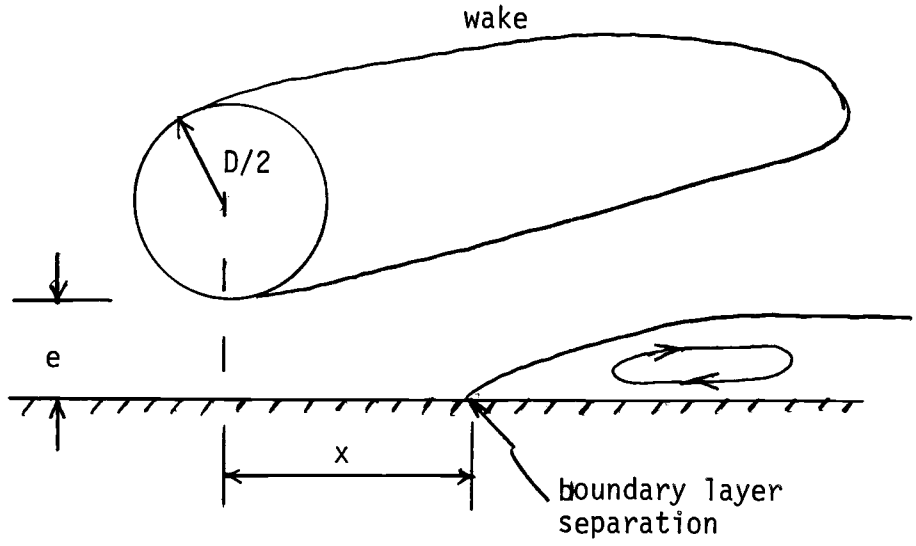

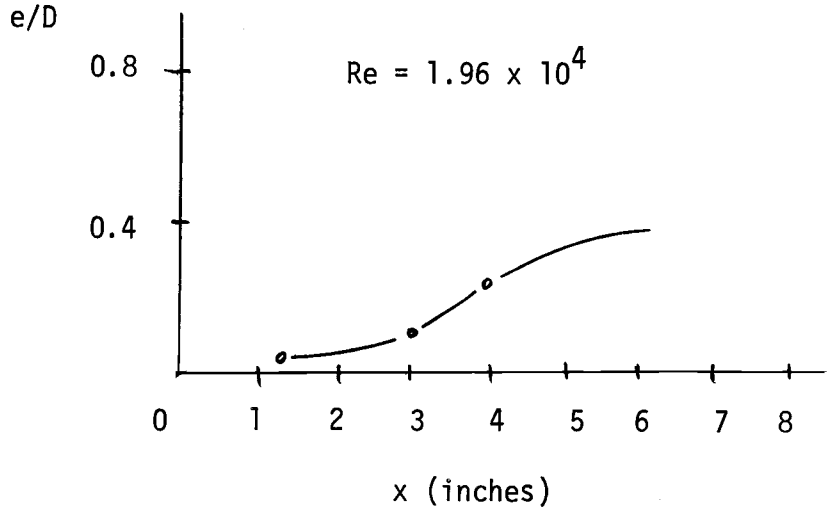

Figure 17 - Channel bottom boundary layer separation point plotted against e/D

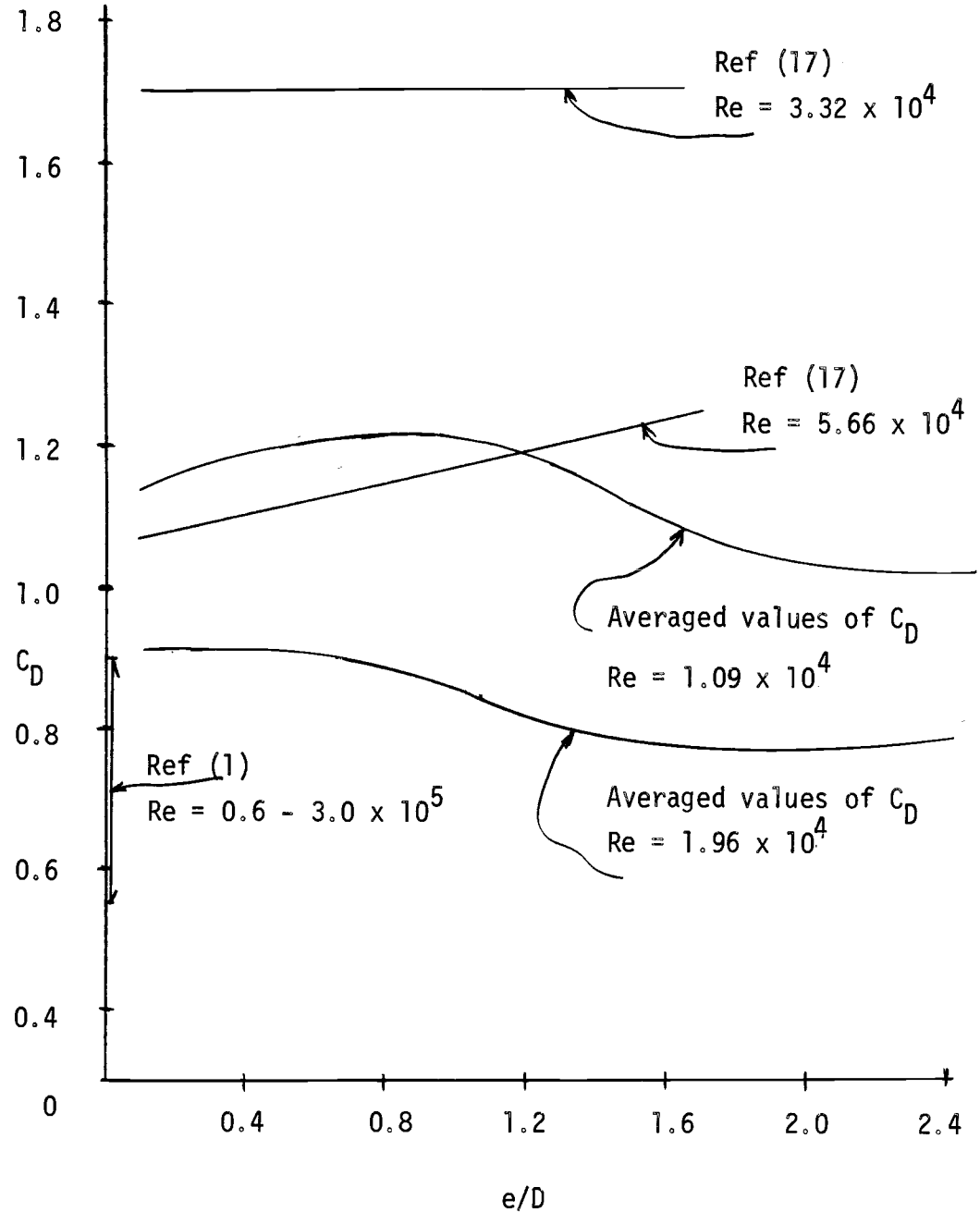

Figure 18 - Comparison between coefficients of drag obtained from previous experimental work, and present experimentation

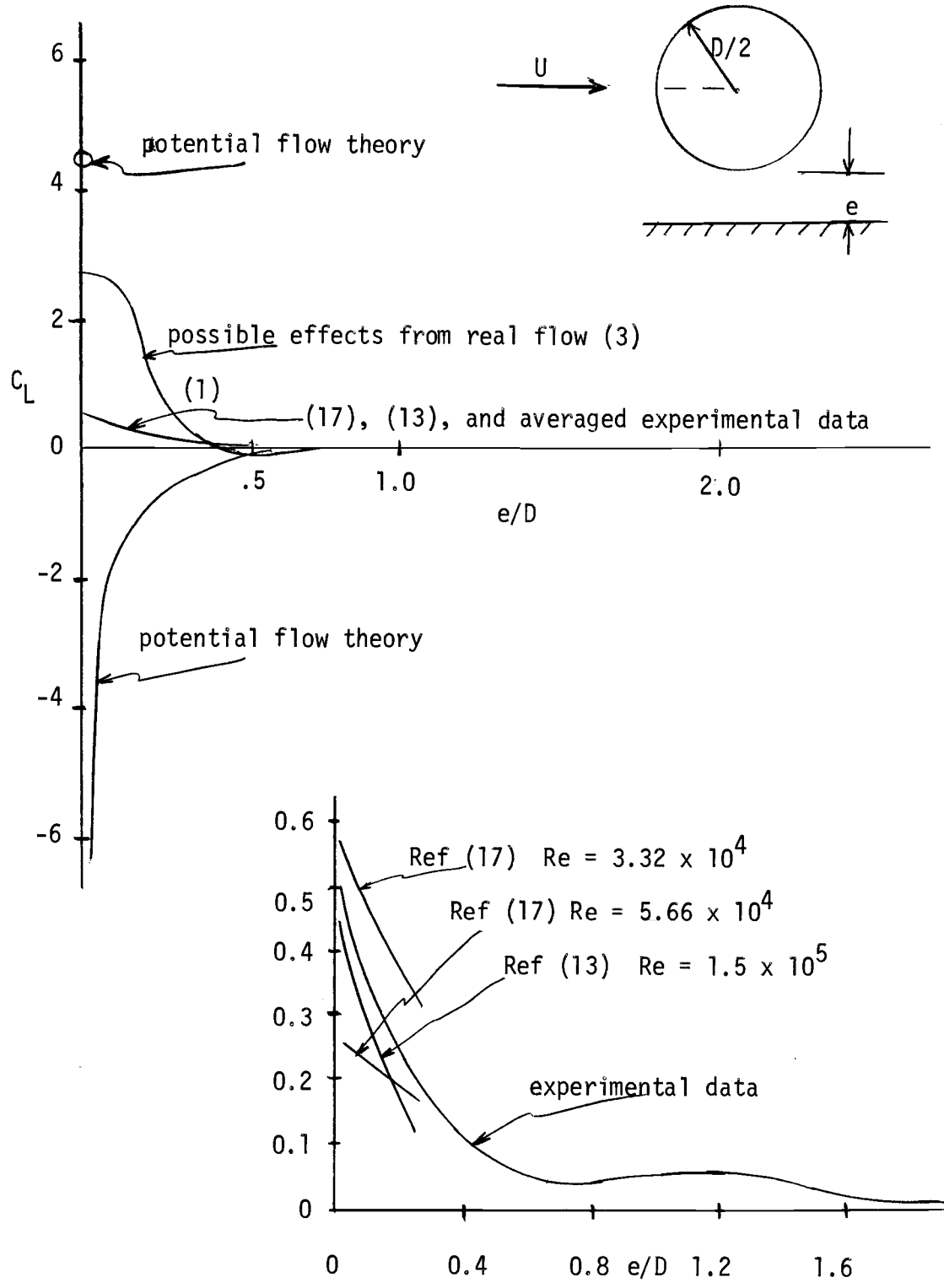

Figure 19 - Comparison between coefficients of lift obtained from previous experimental work, theoretical calculations, and present experimentation

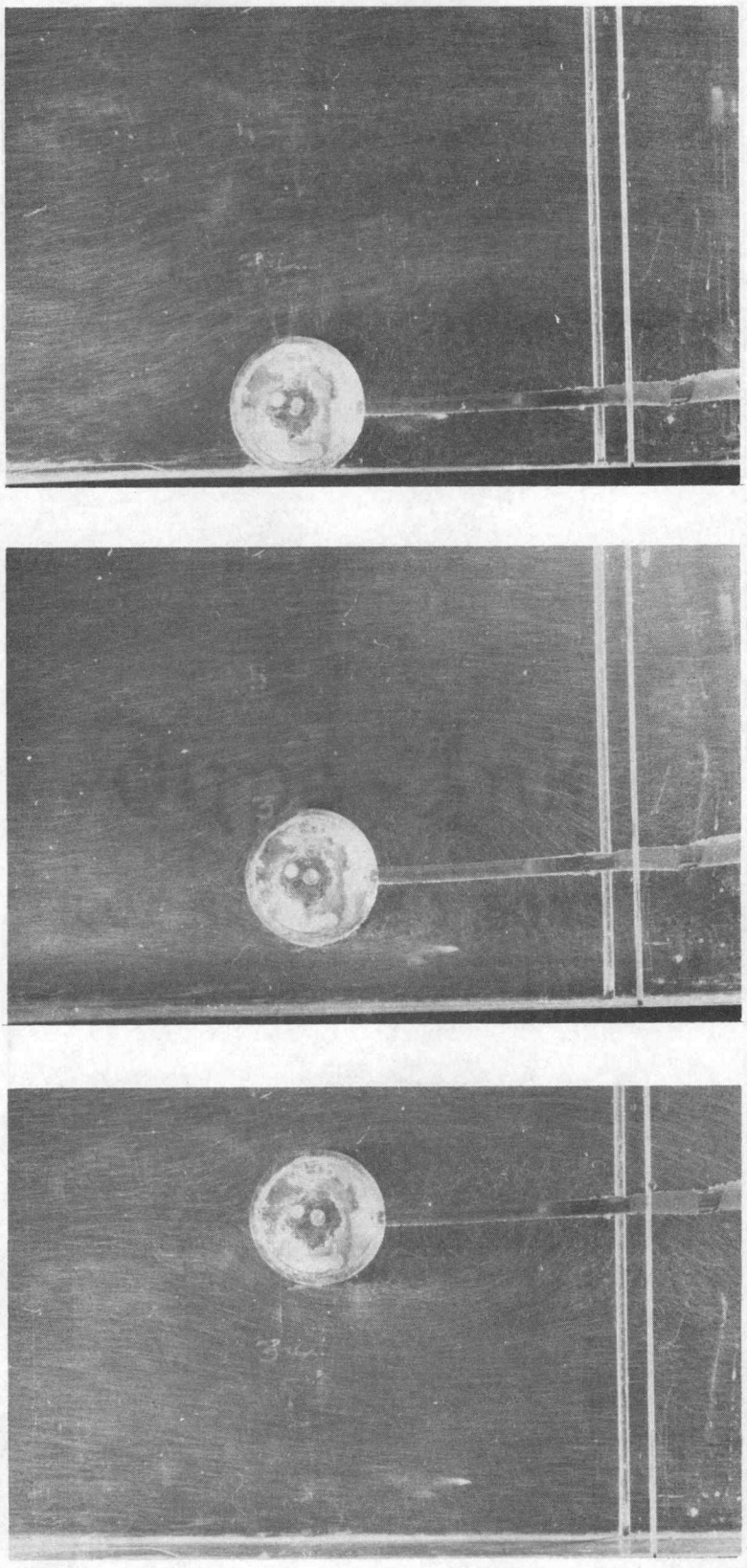

Figure 20 - Visualization of the flow configuration around the cylinder

Figure 21 - Tabulated Data of the Drag Force on the Test Cylinder

a = C_D for Raw Data

b = C_D for Corrected Data*

H = Channel Water Height (ft)

Q = Channel Flow Rate (ft^3/sec)

Run	H	Q		e/D									
				3.00	2.50	2.00	1.50	1.25	1.00	0.75	0.50	0.25	0.125
13	1.33	.315	a	1.21	1.21	1.21	1.24	1.33	1.34	1.37	1.35	1.35	1.35
			b	1.37	1.37	1.37	1.38	1.47	1.48	1.50	1.49	1.48	1.48
14	1.33	.317	a	1.20	1.15	1.15	1.20	1.30	1.37	1.31	1.30	1.44	1.40
			b	1.12	1.05	1.04	1.09	1.18	1.24	1.17	1.29	1.28	1.22
15	1.33	.316	a	1.22	1.20	1.24	1.29	1.42	1.47	1.46	1.31	1.25	1.36
			b	1.20	1.18	1.21	1.25	1.38	1.43	1.42	1.26	1.20	1.31
16	1.33	.316	a	1.30	1.29	1.31	1.36	1.42	1.42	1.47	1.43	1.42	1.4
			b	1.20	1.18	1.23	1.27	1.33	1.33	1.40	1.36	1.35	1.33
17	1.33	.317	a	1.34	1.26	1.28	1.36	1.46	1.40	1.40	1.34	1.28	1.30
			b	1.42	1.35	1.37	1.47	1.56	1.52	1.54	1.46	1.40	1.44
18	1.33	.570	a	1.01	1.01	1.01	0.98		1.03	1.08	1.10	1.14	1.13
			b	1.02	1.02	1.01	0.99		1.04	1.09	1.12	1.16	1.15
19	1.338	.570	a	0.96	0.96	0.95	0.95		1.03	1.09	1.09	1.09	1.10
			b	0.98	0.98	0.98	0.98		1.06	1.12	1.12	1.13	1.13
20	1.338	.570	a	1.00	0.98	0.97	0.94	0.96	1.02	1.06	1.06	1.06	1.08
			b	1.02	1.02	0.98	0.96	0.98	1.04	1.08	1.10	1.10	1.11
21	1.338	.570	a	0.95	0.94	0.92	0.87	0.92	1.00	1.02	1.06	1.07	1.05
			b	1.00	0.98	0.97	0.91	0.97	1.03	1.05	1.09	1.10	1.08

* Correction was made for instrument drift

Figure 22 - Tabulated Data of the Lift Force on the Test Cylinder

H = Channel Water Height (ft) a = C_L for Raw Data

Q = Channel Flow Rate (ft^3/sec) b = C_L for Corrected Data*

Run	H	Q		e/D										
				3.00	2.50	2.00	1.50	1.25	1.00	0.75	0.50	0.25	.125	.03
1	1.338	.357	a	.11	.11	.06	.19	.19	.11	.11	.11	.21	.40	.64
			b	.02	.01	.03	.10	.10	.02	.01	.00	.01	.31	.48
2	1.338	.357	a	.09	.09	.06	.16	.13	.06	.04	.04	.20	.33	
			b	.00	.00	-.01	.10	.06	0.0	-.02	-.02	.15	.27	
3	1.338	.357	a	.04	.06	.09	.13	.16	.20		.22	.40	.83	1.37
			b	.00	.01	.01	.06	.10	.13		.15	.31	.72	1.08
4	1.338	.357	a	.06	.06	.13	.20	.23	.22		.16	.40	.81	
			b	-.03	-.02	.05	.11	.18	.17		.13	.35	.76	
5	1.333	.318	a	-.02	-.02	-.02	-.07	-.08	-.08	.04	.02	.04	.20	
			b	.00	.00	. 0	-.05	-.05	.04	.04	.06	.07	.23	
6	1.344	.315	a	.00	.00	-.03	-.08	-.03	-.06	-.06	-.03	.04	.14	.35
			b	.00	.00	.00	-.07	-.01	-.03	.03	.05	.07	.17	.39
7	1.336	.317	a	.00	.02	.00	-.02	.02	.00	.00	.02	.10	.14	.27
			b	.00	.00	-.01	-.04	-.03	-.02	-.02	.06	.05	.10	.22
8	1.333	.318	a	-.06	-.06	.00	-.10	-.04	-.04	.02	.07	.08	.14	.39
			b	-.01	-.01	.02	-.07	.00	.08	.06	.10	.11	.17	.42
9	1.333	.562	a	-.05	-.03	-.05	.00	.04	-.02	.01	.05	.14	.25	.38
			b	-.01	.01	.00	.05	.09	.03	.07	.11	.21	.31	.45
10	1.333	.562	a	-.04	-.08	-.05	.00	.00	.00	-.01	.01	.15	.24	
			b	.00	-.01	.01	.06	.06	.06	.05	.06	.21	.29	
11	1.338	.570	a	-.06	-.04	-.08	.05	.03	.01	.00	.04	.02	.26	.31
			b	.00	.01	.01	.01	.10	.10	.07	.17	.25	.34	.39
12	1.338	.570	a			-.03	.01	-.01	.01	-.01	.00	.14	.25	
			b			.00	.04	.01	.03	.01	.02	.16	.26	

* Correction was made for instrument drift

Figure 23 - Tabulated Data of the Separation and Stagnation Points of the Cylinder Boundary Layer

$\frac{e}{D}$	Exper. Stag. Pt.	Theor. Stag. Pt.	Exper. Upper Sep. Pt.	Theor. Upper Sep. Pt.	Exper. Lower Sep. Pt.	Theor. Lower Sep. Pt.
0.00	-8.4°		86.0°			
.05		-12.3°		115.2°		-104.2°
.125	-14.0°	-7.2°	89.0°	114.9°		-105.5°
.25	-8.0°	-3.9°	90.7°	114.6°	-97.2°	-107.5°
.50	-3.0°	-1.6°	91.8°	111.4°	-94.8°	-111.5°
.75	-0.5°		95.2°		-93.5°	
1.00	0.0°		94.5°		-91.0°	
1.25	-0.8°		94.0°		-91.5°	
1.50	0.5°		95.0°		-90.0°	
2.00	2.7°		96.3°		-93.0°	
2.50	2.0°	-0.06°	88.5°	111.4°	-88.0°	-111.4°

Exper. = Experimental Stag. = Stagnation

Sep. = Separation Pt. = Point

Theor. = Theoretical

APPENDIX

9.1 - APPENDIX

Computer program for the complex potential, stagnation point, separation point of the cylinder boundary layer

Flow Chart

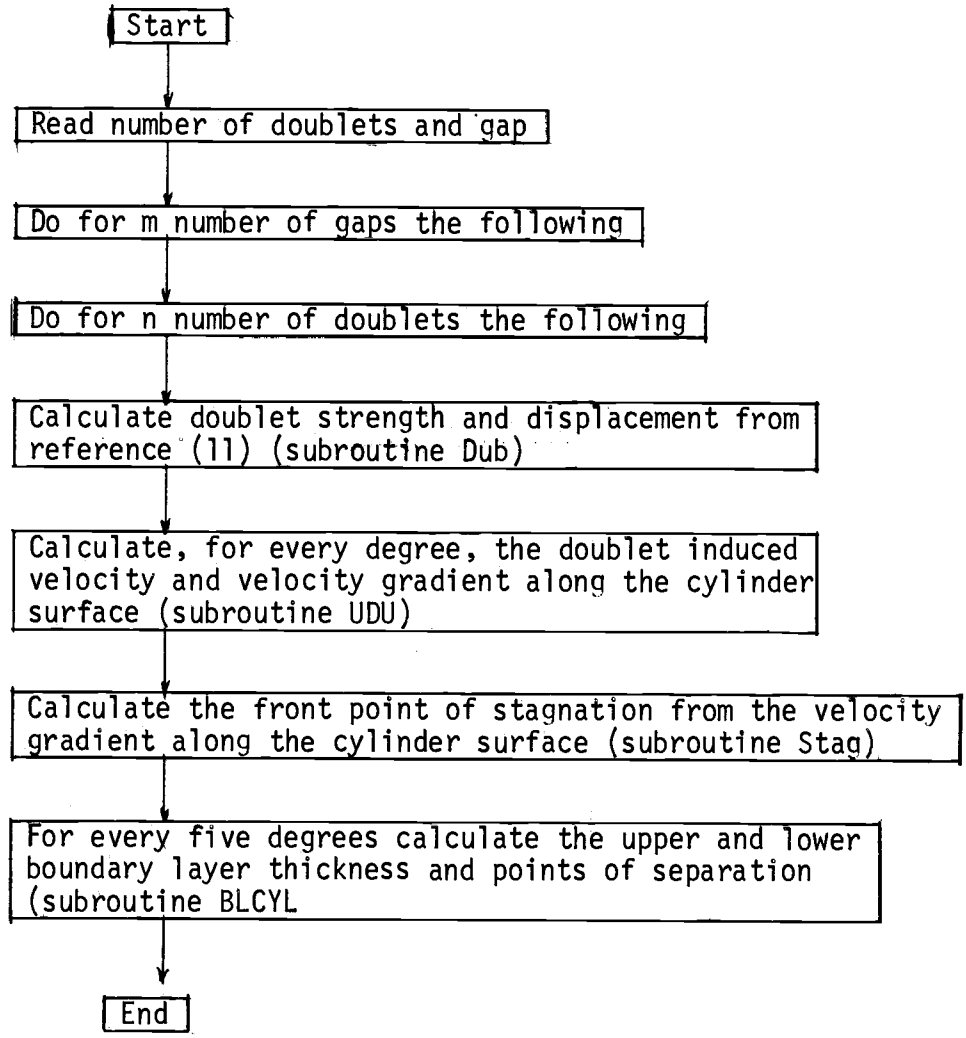

9.2 - APPENDIX

Computer Program for the Complex Potential, Stagnation Point and Separation Point of the Cylinder Boundary Layer.

```
0+001          PROGRAM BLCYL
0+002    CC  BLCYL DETERMINES STAGNATION POINT AND SEPARATION POINT ON
0+003    CC  A CYLINDER NEAR A PLANE BOUNDARY. TCK 2-28-1974.
0+004          COMMON ND,A,E,PI,D(101),B(101),THST,DUST,U,DU,TH,RAM,DTH1,DTH2
0+005    1     CONTINUE
0+006          PI=3.141592653
0+007          READ(60,100) ND,E
0+008          IF(ND.EQ.0) STOP
0+009          WRITE(61,299)
0+010          WRITE(61,200) ND,E
0+011          A=1.0
0+012          CALL DUB
0+013          CALL STAG
0+014          THTST=THST*180./PI
0+015          IST=IFIX(THTST)
0+016          ISTR=IST/5*5
0+017          THTR=FLOAT(ISTR)
0+018          THTR=THTR*PI/180
0+019          DTH2=-5.0*PI/180.
0+020          DTH1=THTR+DTH2-THST
0+021          WRITE(61,201)
0+022          CALL BLAYER
0+023          DTH2=5.0*PI/180.
0+024          DTH1=THTR-THST
0+025          WRITE(61,202)
0+026          CALL BLAYER
0+027          GOTO 1
0+028    100   FORMAT(I5,F12.0)
0+029    200   FORMAT(1H ,3X,≠ ND= ≠,I5,/,3X,≠ E = ≠,E15.7,//)
0+030    299   FORMAT(1H1,≠ STAG. AND SEPAR. POINTS ON CYL. NEAR BOUNDARY ≠,//)
0+031    201   FORMAT(1H ,≠ LOWER PART BOUNDARYLAYER IS***** ≠,/)
0+032    202   FORMAT(1H ,≠ UPPER PART BOUNDARYLAYER IS***** ≠,/)
0+033          END
0+034    CCCCCCCCCCCCCCCCCCCCCCCCCCCCCCCCCCCCCCCCCCCCCCCCCCCCCCCCCCCCCCCCCCC
0+035          SUBROUTINE DUB
0+036          COMMON ND,A,E,PI,D(101),B(101),THST,DUST,U,DU,TH,RAM,DTH1,DTH2
0+037          FL=2.0*(A+E)
0+038          D(1)=1.0
0+039          B(1)=0.0
0+040          DO 10 J=2,ND
0+041          IF(J/2*2.NE.J)GOTO 1
0+042          D(J)=D(J-1)
0+043          B(J)=FL-B(J-1)
0+044          GOTO 10
0+045    1     CONTINUE
0+046          Q=A/B(J-1)
0+047          D(J)=D(J-1)*Q*Q
0+048          B(J)=A*Q
0+049    10    CONTINUE
0+050          RETURN
0+051          END
0+052    CCCCCCCCCCCCCCCCCCCCCCCCCCCCCCCCCCCCCCCCCCCCCCCCCCCCCCCCCCCCCCCCCCC
```

```
          SUBROUTINE UDU
          COMMON ND,A,E,PI,D(101),B(101),THST,DUST,U,DU,TH,RAM,DTH1,DTH2
          SX=0.0
          SY=0.0
          DO 10 I=1,ND
          P=D(I)
          Q=B(I)
          RR=1.0+Q*Q+2.0*Q*SIN(TH)
          PH=ARG(COS(TH),(SIN(TH)+Q))
          X=P*SIN(2.0*PH-TH)/RR
          DPH=((COS(PH)/COS(TH))**2)*(A+Q*SIN(TH))
          Y=P*((2.0*DPH-1.0)*COS(2.0*PH-TH)-2.0*Q*COS(TH)*SIN(2.0*PH
         1 -TH)/RR)/RR
          SX=SX+X
          SY=SY+Y
   10     CONTINUE
          U=SX+SIN(TH)
          DU=SY+COS(TH)
          RETURN
          END
CCCCCCCCCCCCCCCCCCCCCCCCCCCCCCCCCCCCCCCCCCCCCCCC
          SUBROUTINE STAG
          COMMON ND,A,E,PI,D(101),B(101),THST,DUST,U,DU,TH,RAM,DTH1,DTH2
          WRITE(61,400)
          TH=2.0*(PI/180.)
          DTH=-1.0*(PI/180.)
          J=0
    1     CONTINUE
          J=J+1
          TH=TH+DTH
          CALL UDU
          THT=TH*180./PI
          WRITE(61,401) THT,U,DU
          IF(U.LT.0.0) GOTO 2
          IF(J.GE.91) STOP
          CH=U
          GO TO 1
    2     CONTINUE
          THST=TH+DTH*(U/(CH-U))
          TH=THST
          CALL UDU
          P=1.0-U*U
          THT=TH*(180./PI)
          WRITE(61,403)
  403     FORMAT(1H0, ≠ STAGNATION POINT IS....... ≠)
          WRITE(61,402) THT,U,DU,P
          DUST=DU
  400     FORMAT(1H0,≠SEARCH FOR STAGNATION POINT≠,//,
         1 4X,≠ THETA ≠,10X,≠ U ≠,10X,≠ DU ≠,//)
  401     FORMAT(3E12.4)
  402     FORMAT(1H0, 4E12.4,///)
          RETURN
          END
CCCCCCCCCCCCCCCCCCCCCCCCCCCCCCCCCCCCCCCCCCCCCCCC
```

```
      SUBROUTINE BLAYER
      COMMON ND,A,E,PI,D(101),B(101),THST,DUST,U,DU,TH,RAM,DTH1,DTH2
      WRITE(61,502)
      RAM=7.052
      AK=0.0770
      TH=THST
      Z=AK/DUST
      KJ=0
      GOTO 1
2     CONTINUE
      III=0
21    III=III+1
      T1=37./315.-RAM/945.-RAM*RAM/9072.
      FR=T1*T1*RAM-AK
      DT1=-1./945.-2.*RAM/9072.
      DFR=T1*(T1+2.*DT1*RAM)
      RAM=RAM-FR/DFR
      OK=ABS(FR/DFR)
      IF(III.GE.30) GO TO 9
      IF(OK.GT.0.001) GOTO 21
1     CONTINUE
      KJ=1+KJ
      CALL UCU
      T1=37./315.-RAM/945.-RAM*RAM/9072.
      T2=0.3-RAM/120.
      T3=2.0+RAM/6.
      T4=2.0-116./315.*RAM+(2./945.+1./120.)*RAM*RAM+2./9072.*RAM**3
      FK1=T2/T1
      FK2=T3*T1
      FK=2.0*T1*T4
      P=1.0-U*U
      AZ=ABS(Z)
      BLM=SQRT(AZ)
      BLD=FK1*BLM
      BL=BLD/T2
      TAU=2.0*FK2*U/BLM
      THT=TH*180./PI
      WRITE(61,500) THT,U,DU,P,BL,BLD,BLM,TAU,RAM
      IF(KJ.EQ.123) RETURN
      IF(RAM.LT.-12.01) GOTO3
      DTH=DTH2
      IF(KJ.EQ.1)DTH=DTH1
      TH=TH+DTH
      DZ=FK/U*DTH
      IF(KJ.EQ.1) DZ=0.0
      Z=Z+DZ
      AK=Z*DU
      CHE=RAM
      GOTO2
3     CONTINUE
      TH=TH-DTH*(CHE+12.0)/(CHE-RAM)
      WRITE(61,501)
      KJ=122
      GOTO2
9     WRITE(61,503)
503   FORMAT(1H , ≠ TOO MUCH ITERATIONS, STOP. ≠,///)
      GO TO 1
500   FORMAT(9E13.5)
501   FORMAT(1H ,≠ SEPARATION POINT IS***** ≠,//)

502   FORMAT(1H ,3X,≠ THETA ≠,10X,≠ U ≠,10X≠ DU ≠,10X,≠ P ≠,10X,
     1 ≠ BL ≠,9X,≠ BLD ≠,9X,≠ BLM ≠,9X,≠ TAU ≠,7X,≠ RAMDA ≠,//)
      END
CCCCCCCCCCCCCCCCCCCCCCCCCCCCCCCCCCCCCCCCCCCCCCCCCCCCCCCCCCCCCCCCCCC
```

```
0+170          FUNCTION ARG(X,Y)
0+171          ARG=ATAN(Y/X)
0+172          IF(X.GE.0.0)RETURN
0+173          IF(Y.GE.0.0) GOTO1
0+174          ARG=ARG-3.141592653
0+175          RETURN
0+176    1     ARG=ARG+3.141592653
0+177          RETURN
0+178          END
```